(1)

SPECIFICATION FOR AN INFRARED
SATELLITE SURVEILLANCE SYSTEM
FOR THE DETECTION OF AIRCRAFT

THESIS

Timothy J. Lawder
Flight Lieutenant, RAAF

AFIT/GSO/ENP/87D-1

DEPARTMENT OF THE AIR FORCE

AIR UNIVERSITY

AIR FORCE INSTITUTE OF TECHNOLOGY

Wright-Fatterson Air Force Base, Ohio

88 3 01 173

SPECIFICATION FOR AN INFRARED
SATELLITE SURVEILLANCE SYSTEM
FOR THE DETECTION OF AIRCRAFT

THESIS

Timothy J. Lawder
Flight Lieutenant, RAAF

AFIT/GSO/ENP/87D-1

DTIC
ELECTE
MAR 0 2 1988

H

AFIT/GSO/ENP/87D-1

SPECIFICATION FOR AN INFRARED SATELLITE

SURVEILLANCE SYSTEM FOR THE

DETECTION OF AIRCRAFT

THESIS

Presented to the Faculty of the School of Engineering

of the Air Force Institute of Technology

Air University

In Partial Fulfillment of the

Requirements of the Degree of

Master of Science in Space Operations

Timothy J. Lawder, B.E.

Flight Lieutenant, RAAF

November 1987

Preface

The purpose of this study was to develop a methodology for designing a specification for an infrared satellite surveillance system for the detection of aircraft against a background of the earth. Very little actual performance data has been presented, in order for this report to be presented at an unclassified level. This report deals with the detection system and is not concerned with other satellite hardware or the data processing system.

I would like to acknowledge the assistance I have received in completing this thesis. I am deeply indebted to my thesis advisor, Lt. Col. Howard Evans, whose invaluable assistance enabled this thesis to be completed. I also wish to thank Dr. Joe Cain for his assistance in completing the Life Cycle Cost methodology section. Finally, I wish to thank my family for their understanding during the hours I spent working on this thesis.

Timothy J. Lawder

ii

Table of Contents

List of Figures

List of Tables

AFIT.GSO/ENP/87D-1

Abstract

This report gives a methodology for designing an infrared satellite surveillance system for detection of aircraft against a background of the earth. Values for target intensity and background radiance have been assumed, and a satellite detector focal plane array configuration has been designed. System calculations have been performed and indicate that detection of aircraft against a background of the earth appears feasible. This report contains limited actual data due to its unclassified level.

SPECIFICATION FOR AN INFRARED SATELLITE SURVEILLANCE

SYSTEM FOR THE DETECTION OF AIRCRAFT

I. Introduction

General Background

Satellite-based infrared sensors are currently used for detection of ballistic missile launches and for earth surface imaging. Due to the size, motion and relatively small thermal emission of aircraft, construction of a system to detect aircraft from a satellite has yet to be accomplished.

Teal Ruby is an infrared aircraft detection experiment currently being conducted by Rockwell International under the sponsorship of Defense Advanced Research Projects Agency (DARPA). Its goal is to evaluate the feasibility of aircraft detection from a satellite. The satellite is ready to be launched but is currently delayed awaiting a suitable launch vehicle.

Teal Ruby is a developmental system; however, it is not intended to be a prototype for an actual operational system. It is concerned only with the infrared detection process and does

1

not consider the whole of a threat warning system, which would include orbits and satellite constellations, ground stations and communications, and data processing and control.

Development of a satellite-based infrared aircraft detection system to operationally carry out a specific purpose has not yet been completed and requires investigation. Discussions with the Directorate of Communications-Electronics (DCE-AF) staff at the Australian Department of Defence (Air Force) in May 1986 identified aircraft detection from satellites as a suitable research project.

Design of an actual operational system would have to be carried out around a specific ground area, and the region selected for this project, from 120 degrees E to 150 degrees E and from the Equator to 15 degrees S, is just an example. The ground area selected, which includes the northern Australian coast, is a sample region selected by the author, and does not reflect the views of the Australian Government or the Royal Australian Air Force. The methodology used for the system design would be similar for any other ground area.

Specific Problem Statement

A system is required to detect aircraft as they fly over the region from 120 degrees E to 150 degrees E and from the Equator

to 15 degrees S. The detection system is to use infrared detection and be satellite based. The proposed solution will cover all aspects of the detection system except for satellite hardware. Actual sensor design will be limited, with only a specification being provided for the detectors.

Due to the many classified aspects contained in the Teal Ruby project, and as this research problem is being kept at an unclassified level, the proposed system may differ appreciably from the Teal Ruby developmental system.

Subsidiary Questions

The following is a list of major research questions which must be answered in order to specify the complete system. While these questions are listed separately, they are not necessarily independent.

1.   What are the typical aircraft infrared emissions, both from the aircraft skin and exhaust plume, which the system would be expected to detect ? (chapter 4).

2.   What are the typical backgrounds that the targets will have to be compared against ? (chapter 4).

3.   What attenuation through the atmosphere could be expected over the region selected ? (chapter 5).

3

4.   What is the optimal orbit for the satellites ? (chapter 6).

5.   What is the optimal satellite constellation ? (chapter 6).

6.   What are the sensor requirements ? (chapter 7).

7.   What is the methodology for calculating the life cycle costs
for the system ? Limited detail on the system that will be
proposed will be provided in this area due to the lack of
information on satellite hardware. (chapter 9).

II. Background

Three areas applicable to this thesis are discussed in the following sections. They are the Teal Ruby experiment, detector arrays and charge coupled devices, and staring sensors. These areas set the groundwork from which this thesis evolved, and the discussions provide a background which will be amplified in the chapters dealing with that subject.

Teal Ruby

As outlined in the introduction, Teal Ruby is an infrared aircraft detection experiment. It is an advanced, earth orbiting sensor developed to demonstrate the ability to detect airborne vehicles from space using new generation (at the time of design) infrared mosaic technology, and to provide an extensive target and background data base. The Teal Ruby sensor consists of a cryogenically cooled, infrared staring mosaic focal plane array sensor mounted in a telescope, utilising infrared charge coupled device type detector arrays.

The Teal Ruby program has three major objectives (16:25):

1. To demonstrate the feasibility of aircraft vehicle detection (AVD) from space with an infrared mosaic sensor.

5

2. To demonstrate the requisite technologies and to assess the performance changes of infrared focal plane arrays over long periods of time in space.

3. To generate and establish a data base of radiometric and other data that will support the development and test of future AVD sensors and space surveillance systems.

During a typical test of the Teal Ruby system, the sensor may be pointed at a particular area on the earth's surface, and its field of view will stare at that area as the satellite passes. The sensor telescope will rotate on a yoke and spindle mechanism attached to the side of the spacecraft to compensate for satellite movement.

For aircraft flight detection, aircraft will be scheduled to fly across the field of view as the sensor observes the area to test the sensors ability to detect aircraft movement across the stationary background of infrared return. On board processing capability of the system is designed to remove the infrared background clutter received by the sensor from topographical features the aircraft is flying over (17:8).

The Teal Ruby gimbaled sensor contains the telescope, the mosaic focal plane and the cryostat. The cryostat maintains the focal plane detectors below 16 degrees Kelvin. The expected

6

lifetime of the Teal Ruby experiment is one year, the time for the supply of cryogens for cooling the detectors to be depleted.

The focal plane has 11 separate spectral bands ranging from short wave to long wave infrared. Each filter is selected for a particular set of experiments. Each of the 11 spectral bands contains 12 CCD chips arranged in a 3 x 4 chip zone. Each chip contains an array of pixels (pictur elements). A single zone is therefore a mosaic, which when pointed and stabilised over an area on the earth's surface, presents a mosaic footprint on individual picture elements. A pixel integrates the in-band energy during a time interval of 1 to 1000 milliseconds depending on the infrared in-band power level being received by that zone (16:62).

The telescope has a 2.25 degree total field of view about the central ray of the optics and has a pointing capability which positions this central ray (line of sight) with respect to inertial space in both intrack and crosstrack directions as referenced from the principal spacecraft axes.

Due to the classified nature of the Teal Ruby sensor design and performance, information on the sensor was unavailable at an unclassified level.

Arrays and Charge Coupled Devices

Increasing detector performance is becoming very difficult as the theoretical performance limits of the detectors are approached. The next logical step is to increase the number of detectors in an array. The objective of focal plane array technology is to satisfy the requirement for larger arrays by means of the integrated circuit approach. The goal of this approach is to perform all necessary functions, prior to signal processing, on the same chip (12:183).

The two major advantages of focal plane arrays are (12:184):

a. They provide an economical method for high density packing of the focal plane array; and

b. They allow signal processing to take place on the focal plane.

With a large number of detectors, the most practical way to read the information from the individual detectors is by multiplexing: bringing out the data in serial streams through a number of time shared elements. This charge transfer is made possible by using a Charge Coupled Device (CCD).

The CCD, invented by Boyle and Smith (3) in 1970, is a metal oxide semiconductor (MOS) structure that can collect and store

8

charge packets from a detector in localised potential wells. The CCD permits charges collected at individual detector elements to be transferred in a linear fashion from CCD well to CCD well to the end of the array where they can be read out (15:61).

The CCD is divided into a large number of pixels (picture elements), each corresponding to a location on the final image. The pixels are arranged into columns separated by an insulator. After a picture is taken, the collected electrons in the pixels in each column are read out by passing them along the column to an external circuit which feeds them to a computer. A pixel then has two functions. As well as trapping the electrons freed by incoming photons of light, it must be able to transfer this charge to the next pixel up the column, while simultaneously picking up the charge from the adjacent pixel down the column. The transfer of charge in this way gives the device its name (8:49).

Detector Materials and Construction

There are two broad categories of Infrared Charge Coupled Devices (IRCCDs), monolithic and hybrid devices. In the monolithic IRCCD, the infrared sensitive substrate is either a narrow bandgap semiconductor or an extrinsic semiconductor with appropriate impurity ionization energy. The hybrid IRCCD consists

of the coupling of an infrared detector to a standard silicon CCD unit (19:621,.

Monolithic CCDs should be the more economical and effective as both detector and CCD are on the same substrate. Hybrid CCD focal planes allow the detector array and CCD to be optimised independently and tested before they are assembled together, which improves the yield (9:691).

According to Tebo, the Mercury-Cadmium-Telluride (HgCdTe) semiconductor alloy has established itself as the most widely used high performance infrared detector (20:72). HgCdTe is used in both the monolithic and hybrid approaches. The monolithic approach confines the function of infrared detection and charge transfer to within the HgCdTe alloy, while the hybrid approach mates the HgCdTe alloy to a silicon CCD.

Kruer, Scribner and Killiany (12:183) state that the Navy is currently developing arrays in HgCdTe for the following reasons:

a.   The ability to detect radiation in both the 3 to 5 micrometre and 8 to 12 micrometre wavelength bands;

b.   The ability to select cutoff wavelengths by changing the alloy composition of the material;

c.   The availability of high quality bulk substrate;

d.   The availability of epitaxial growth technology; and

e.   The potential for higher temperature operation.

Consequently, Kruer, Scribner and Killiany state (12:187) "The
DoD has made HgCdTe the material of choice for infrared focal
plane technology".

By varying the composition of the HgCdTe alloy, the
wavelength response can be peaked anywhere in the range 2-25
micrometres. Jamieson (9:691) states these detectors can also
have a high quantum efficiency, high response speed, and can
operate at temperatures of 70 to 140 degrees K (compared with
operating temperatures of 12 to 20 degrees K for other
detectors). Even as early as 1979, Lloyd stated (15:93) " HgCdTe
will be used for high background, space surveillance
applications." This opinion is supported by Chan, who states that
hybrid arrays using HgCdTe alloys are in current fashion and will
be used more in the future (5:698).

Staring Sensors

Space based sensors that search for targets close to the
earth must be able to discriminate the targets' emissions from
those of background features such as clouds, nonuniformity in
terrain, contrasts between water and terrain, etc. These clutter
signals from irrelevant features are often more likely to cause
false alarms and missed detections than random noise (9:692).

The application of staring infrared sensors are ideal for this case as they offer better tracking accuracy and improved signal to noise performance (17:44). A staring sensor has a two-dimensional mosaic detector array with one detector assigned to each pixel of the field of view currently under surveillance, compared to a scanning sensor which has a one-dimensional array of detectors that scans systematically over the field of view.

The performance advantages of a staring sensor include greater sensitivity because of a longer integration time (time to collect the emitted energy), improved background clutter rejection through signal processing to allow the detection of smaller targets, an ability to detect very short duration events, and no time lag as the entire field of view is always being sensed (7:91).

Scanning sensors use relative intensity to reject the background as the targets that are detected are brighter. Staring sensors can detect dimmer targets as they do not operate solely on relative intensity but also use background suppression. The sensor uses the fact that radiation from natural backgrounds varies slowly with respect to time and space compared to the changes in a moving target (16:85). A sensor can also be operated in a step staring mode, where it will stare at a field of view for a set amount of time, then move on to another field of view and stare.

Staring sensor arrays generally require a very large number of detectors (approximately 1-10 million), each of which is assigned a field of view of less than .05 degree. According to Schultz and Russell, as many as 100,000 monolithic type detectors per square inch can now be fabricated, with production yield rates and reliability levels approaching 95 percent (17:47).

III. Methodology

This chapter outlines the methodology which could be used to develop the infrared aircraft detection system. The system design is divided into separate phases, and these phases are illustrated in Figure 1. Discussion on these phases is included in the chapters as noted on Figure 1. The methodology used for each phase is discussed below.

Detection Requirements

Information on possible targets and background can be obtained and this information used to calculate target intensity and background radiance. Detection requirements are discussed with resolution cells and track files defined. Calculation of actual resolution cell size is performed in Chapter 7.

Atmospheric Absorption

Calculation of the atmospheric absorption factor for this system can be done using LOWTRAN6, an atmospheric transmission computer package. The atmospheric transmittance, as a function of wavelength, is calculated and these data, combined with target intensity, can be used to calculate the optimum operating wavelength.

GROUND STATION REQUIREMENTS

DATA PROCESSING

SATELLITE HARDWARE

LIFE CYCLE COSTS METHODOLOGY

CHAPTER 9

SYSTEM CALCULATIONS

CHAPTER 8

CONCLUSIONS AND RECOMMENDATIONS

CHAPTER 10

SATELLITE OPTICS DESIGN

CHAPTER 7

SATELLITE FOCAL PLANE ARRAY

CHAPTER 7

ATMOSPHERIC ABSORPTION

CHAPTER 5

SATELLITE ORBITAL CHARACTERISTICS

CHAPTER 6

NUMBER OF SATELLITES

CHAPTER 6

TARGET DETECTION REQUIREMENTS
- RESOLUTION
- TIME BETWEEN DETECTIONS
- TRACK FILE

CHAPTER 4

TYPICAL TARGETS AND BACKGROUNDS

CHAPTER 4

GROUND AREA COVERAGE

CHAPTER 1

REQUIREMENT TO DETECT AIRCRAFT OVER GROUND AREA
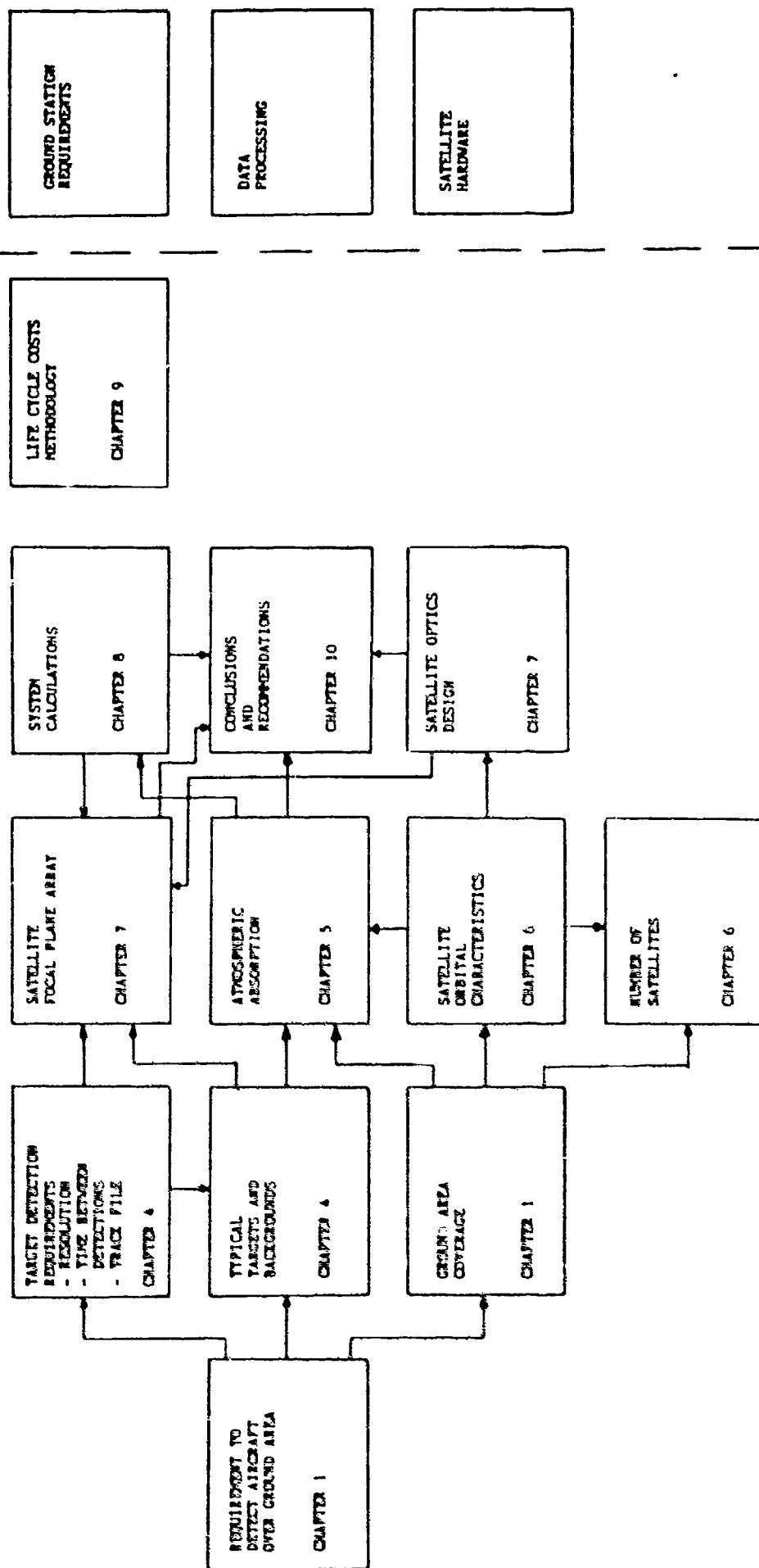
CHAPTER 1

Figure 1. Methodology Phases

15

Satellite Orbital Characteristics

Satellite orbital parameters are discussed, and orbits and satellite field of view are defined. Optimal satellite altitude can be calculated. This altitude is a tradeoff between satellite received irradiance and satellite optical parameters.

Satellite Focal Plane Array

Working from a designated focal plane array size and an estimated number of pixels, ground resolution cell size can be determined. This information, combined with probabilities of accurate detection, can be used to calculate the satellite optics requirements. Sca .ning method and focal plane array layout can be designed, and these are a function of time between detections and integration time.

System Calculations

This chapter presents the equations for calculating satellite received target current and background current, as well as the maximum integration time. Signal-to-noise equations are also presented. Due to the number of uncertainties in this system, these equations have not been evaluated but are presented to enable calculation if suitable data is available.

Life Cycle Costs

Due to the number of uncertainties in this system and the
fact that this design does not consider the whole satellite
system, the life cycle costs (LCC) have not actually been
calculated. The methodology for calculating the LCC is presented,
and can be performed if suitable data is available.

IV. Detection Requirements

Targets

As the infrared signature characteristics for most military aircraft is classified, approximations have been made about a typical aircraft infrared signature. Due to this lack of unclassified information, this analysis will only be concerned with one aircraft and will not offer a comparison between detectability for different aircraft.

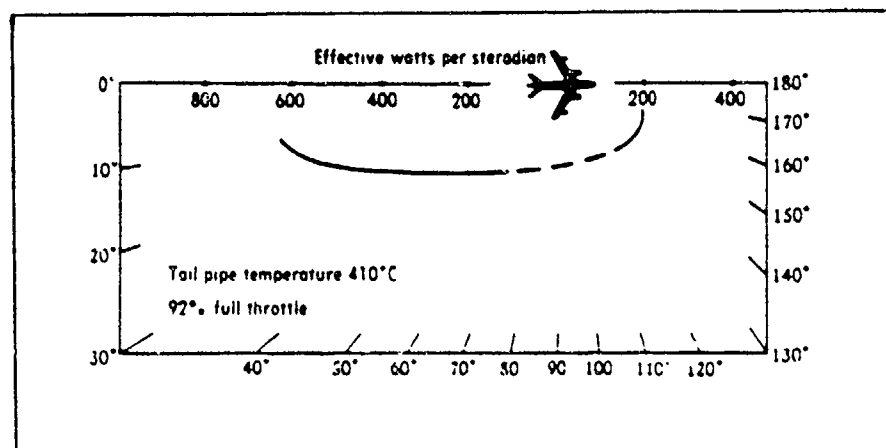Boyd (2:21-14) details a radiation pattern for a B-52 aircraft, which is illustrated in Figure 2.

Figure 2. B-52 Radiation Pattern (2:21-14)

This figure illustrates the intensity within the 2 - 2.6 micrometre wavelength region and includes adjustments for atmospheric absorption and optical filter transmission from the sensor. Using Figure 2 and by approximating an overhead view (from a satellite) to equate to the view from an angle of 40 degrees azimuth, an aircraft intensity of 300 Watts/Steradian can be estimated. As this figure assumes some atmospheric absorption and optical filter loss, the actual aircraft intensity would be higher in this wavelength band.

The tailpipe temperature of the B-52 aircraft has been measured at 410 degrees C (683 degrees K). Wien's displacement law specifies the wavelength where the Planck blackbody function reaches its maximum value. The equation is (18:100)

$$\lambda_{max} T = 2897.8 \tag{1}$$

where λ_{max} is the wavelength (μm)

T is the temperature ($^\circ K$)

For 683 degrees K, the maximum blackbody emission occurs at 4.25 micrometres.

Since this measurement was taken over the 2 - 2.6 micrometre region, and as the peak emission is at 4.25 micrometres, a higher

19

intensity would be emitted at a wavelength nearer 4.25
micrometres. Figure 3 is a graph of the normalized blackbody
emission, as a function of wavelength, for an object at 683
degrees K. From Figure 3 and assuming a detector operating
wavelength of approximately 4 micrometres (operating wavelength
will be discussed in Chapter 5), the aircraft target intensity
would be approximately 3 times the intensity compared with the
intensity if the wavelength was in the 2 - 2.6 micrometre band.
An aircraft target intensity of 900 Watts/Steradian has been
estimated and will be used for the remainder of this report. It
has also been assumed that the intensity is constant over all
viewing angles.
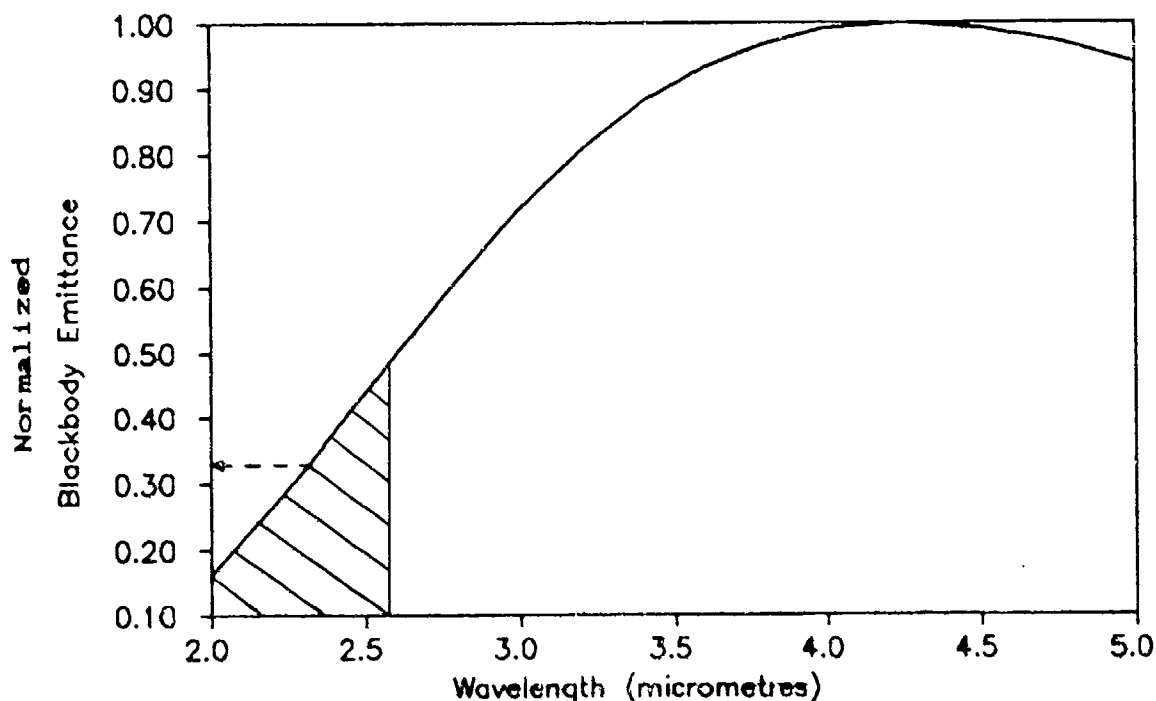
Figure 3. 683 degrees K Blackbody Emission

Due to the long range that an aircraft has to travel to approach Australia from the northern direction, the aircraft would be likely to be flying at a high altitude and not at its maximum speed. For the purposes of this report, the aircraft is assumed to be flying at 30000 ft (approximately 10 kilometres) and travelling at a speed of 500 knots (nautical miles/hour).

Detection Backgrounds

The ground area that would be a background against which targets are to be detected contains desert (sand), water and tropical forest. Typical figures for the reflectance of these backgrounds (at a wavelength of 4 micrometres) are (21: 3-44,3-90),(4:554-569):

Sand	R = 0.35
Forest	R = 0.1
Water	Refer Figure 4
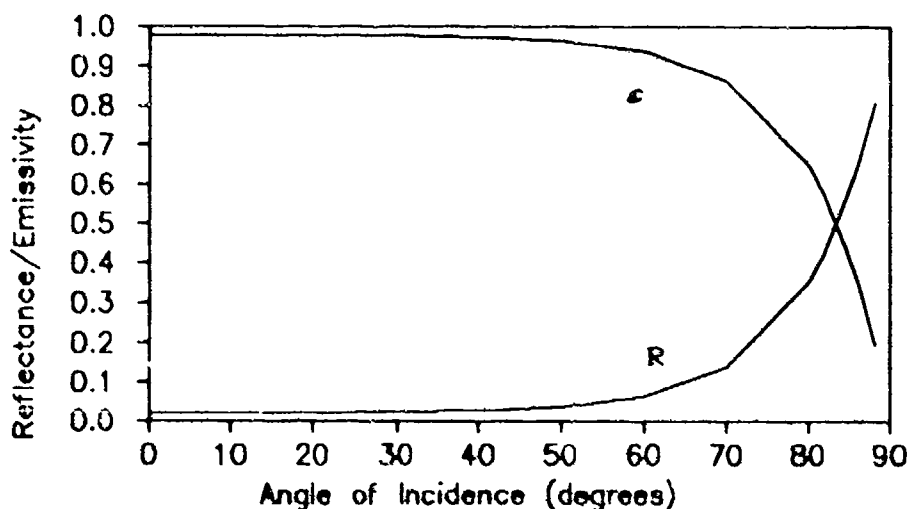
Figure 4. Reflectance of Water

21

Plotted in Figure 5 is the "zone of confusion" region which compares the radiance of reflected sunlight from the earths surface to the radiance of the thermally emitted flux from the earths surface. These figures have been calculated using a sun temperature of 5800 degrees K, an earth temperature of 303 degrees K, and an angle of incidence of 50 degrees. Reflectance and emissivity figures used were for water and were obtained from Bramson (4:551-577).
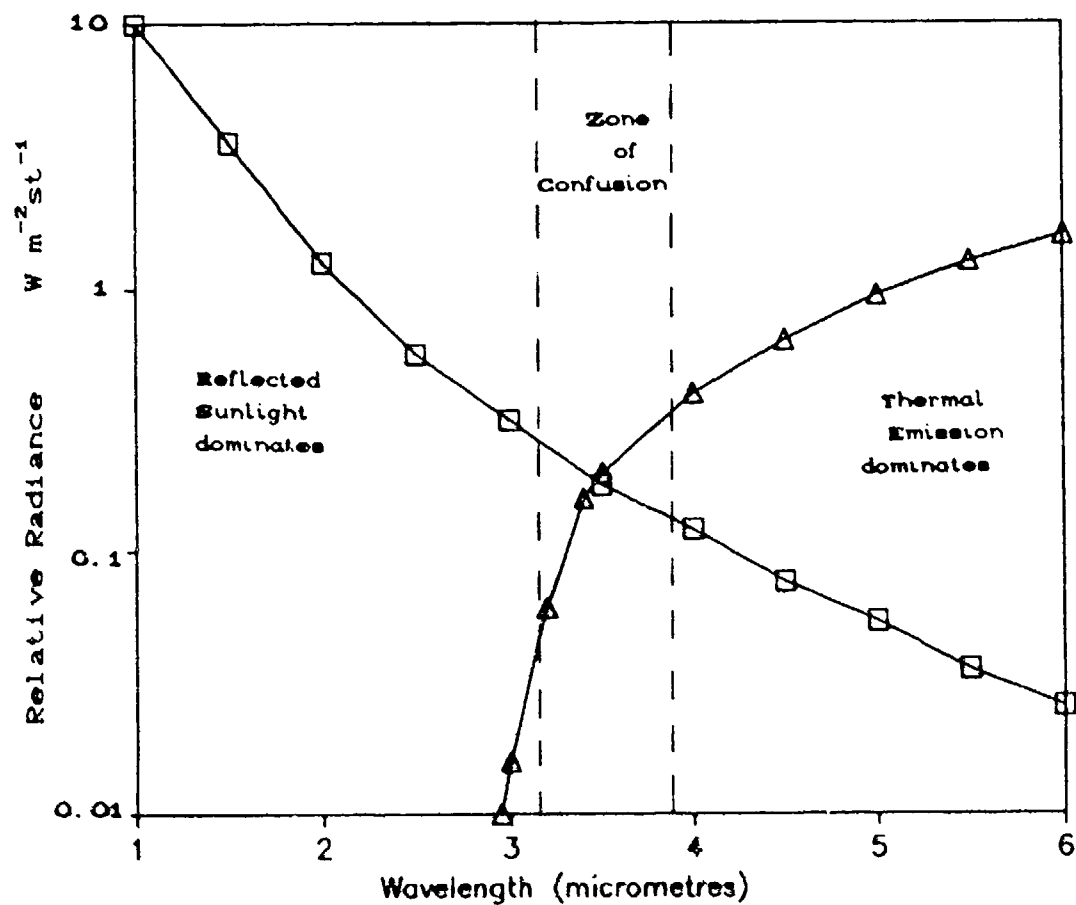
Figure 5. Wavelength Zone of Confusion

This graph illustrates that for any wavelength above 3.5 micrometres, thermally emitted flux is dominant and the reflected sunlight can be neglected.

As the emissivity of water appears to be greater than for other backgrounds, its characteristics will be used for the remainder of this report (in effect, assuming worst case conditions). Accurate figures for the emissivity of water, as a function of both angle of view and wavelength, are detailed in Bransom (4:554-566).

Detection Requirements

The purpose of this section is to outline the requirements for a successful detection and the parameters that would be deemed acceptable to a controller to report the aircraft as a probable target. These figures are only examples, and for an actual system, they would be specified by the controlling authority.

The speed of the target has been estimated to be 500 knots (0.257 km/sec). If it traversed the entire region (from the equator to 15 degrees S), the flight time would be 108 minutes (if travelling South). Specification of an acceptable resolution cell within the region is required. Table 1 lists various

23

resolution cell sizes and the times for an aircraft to fly across
that cell.

Table 1. Resolution Cell Size and Aircraft Flight Time

Resolution Cell Size (km)	Aircraft Flight Time (seconds)
5	19.5
4	15.6
3	11.7
2	7.8
1	3.9

As the size of the resolution cell depends on the number of
detectors that can be placed in the satellite focal plane array,
a minimum requirement of a 3 km resolution cell is considered
acceptable for aircraft placement. This is due to the size of the
ground area being covered and a track file would be established
on an aircraft to allow for more accurate location.

As an aircraft would be flying over a resolution cell for a
maximum time of approximately 12 seconds, it would not be
necessary to have the detector point at the cell for the whole
time. Therefore, an acceptable time between observations would
need to be specified. Assuming that two successful detections

24

would be required within each resolution cell, a maximum time between detections of 5 seconds appears reasonable.

In order to establish the direction and a more precise location for the aircraft, a track file would need to be established. Referring to Figure 6, detection across three to four resolution cells would give more detailed information about an aircraft's direction and location.

Figure 6. Possible Aircraft Track Files

The following parameters are being utilised in this report
to establish a satisfactory target detection track file:

Resolution Cell   -less than 3 km
Time Between Detections   -less than 5 seconds
Track File   -more than three resolution cells

V. Atmospheric Absorption

Atmospheric absorption and scattering has a very strong effect on the received irradiance at a satellite when a target is in the atmosphere or being viewed against a background of the earth. As the aircraft this system is being designed to detect will be flying in the atmosphere against a background of the earth, the effects of atmospheric transmission have to be analyzed.

The atmospheric transmission calculations have been completed using a Fortran Computer code, LOWTRAN6, developed by the Air Force Geophysics Laboratory (AFGL). The LOWTRAN code calculates atmospheric transmittance and radiance over the wavelength region 0.25 to 26.5 micrometres. The code uses a single parameter band model for molecular absorption, and includes the effects of continuum absorption, molecular scattering, and aerosol extinction. Refraction and earth curvature are included in the calculation of an atmospheric slant path.

The code contains representative atmospheric and aerosol models and the option to replace them with user-derived or measured values. Other relevant features of the code include a wind dependent maritime aerosol model, a vertical structure aerosol model, a cirrus cloud model and a rain model (i1:10). For this system, the maritime aerosol model and the cirrus cloud model

27

optimum have been used. Appendix A lists the instructions for using LOWTRAN6, and includes the input parameters used.

Figure 7 is the atmospheric LOWTRAN 6 calculated transmittance along a vertical path from the earth's surface to a satellite in space, as a function of wavelength. The data was obtained using a tropical model atmosphere with a maritime aerosol profile.

Figure 8 illustrates the relationship between satellite altitude (h) and the atmospheric zenith angle (a). Figure 9 is the atmospheric transmittance as a function of zenith angle (for a slant path to space), assuming a wavelength of approximately 4 micrometres.

As the target will be flying at an altitude of approximately 10 km, the atmospheric transmittance for the target will be different from the atmospheric transmittance for the background. Figure 10 illustrates the atmospheric transmittance as a function of wavelength, measured from a target at an altitude of 10 km vertically to a satellite in space (compare to Figure 7). Figure 11 is the atmospheric transmittance for the target as a function of zenith angle (compare to Figure 9).
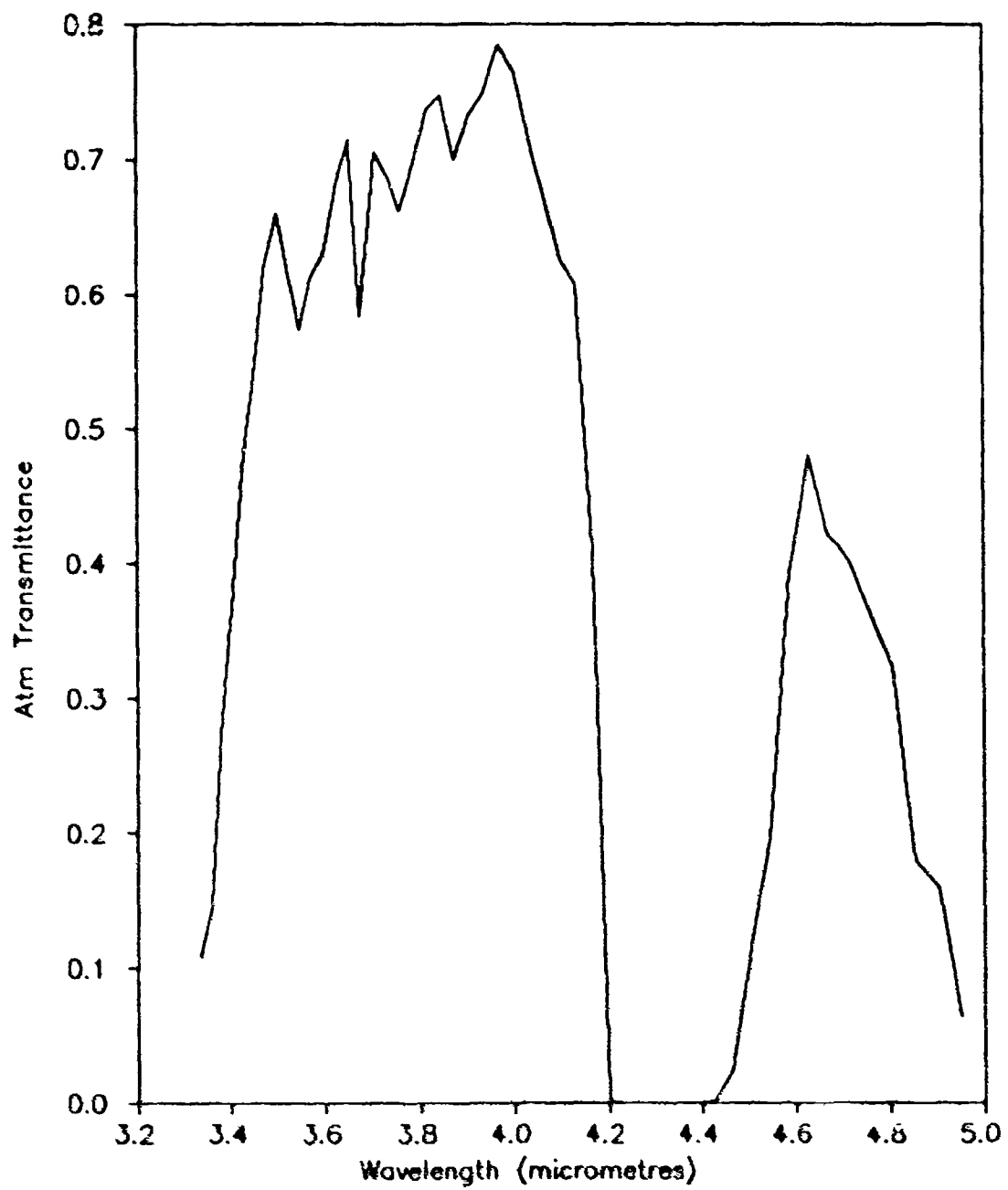
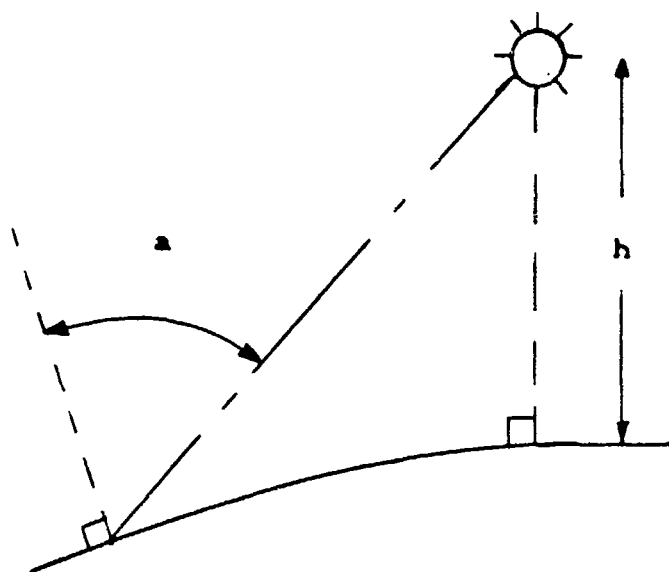Figure 7. Atmospheric Transmittance from earth's surface to space

29

Figure 8. Satellite Altitude versus Zenith Angle
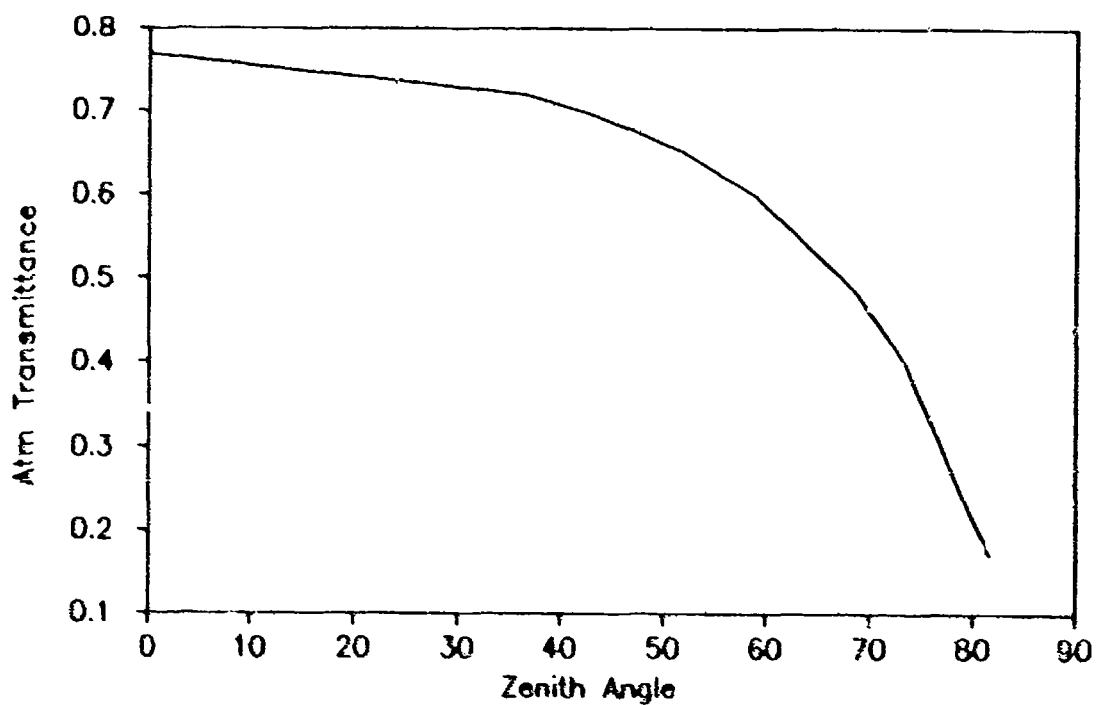
Figure 9. Atmospheric Transmittance from the earth's surface

as a function of Zenith Angle

30
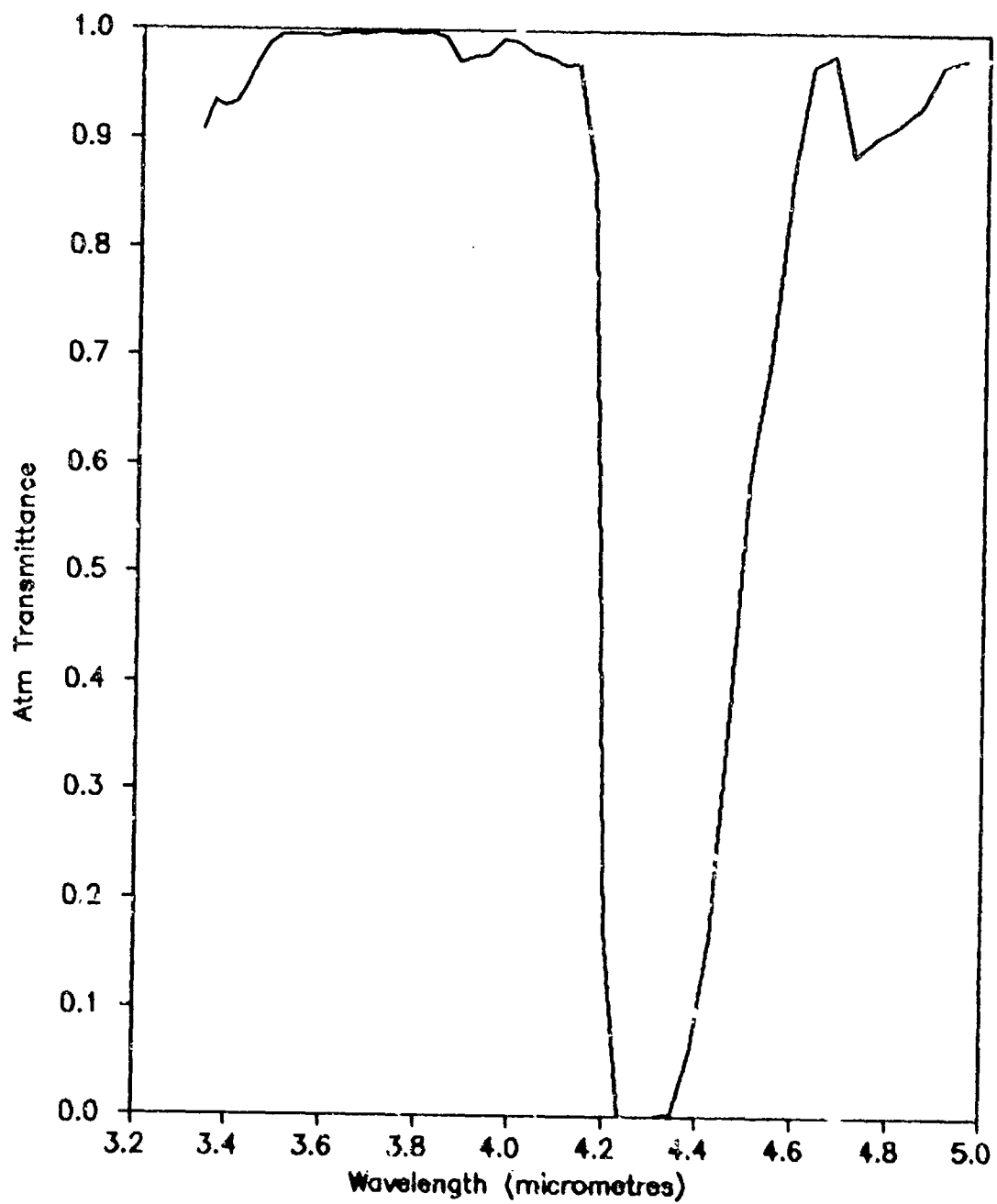
Figure 10. Atmospheric Transmittance from 10 km to space
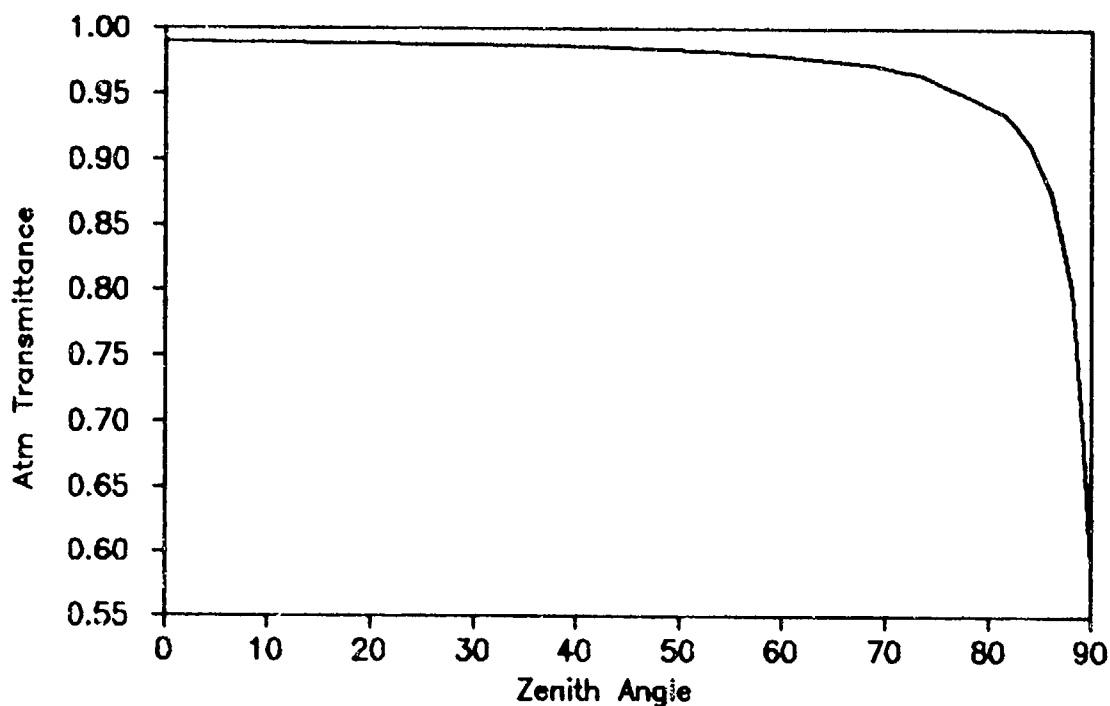
Figure 11. Atmospheric Transmittance from 10 km as a function of

zenith angle

Cirrus Clouds

Cirrus clouds are an important consideration in the
atmospheric transmittance for this system due to their presence at
high altitudes. The distinguishing characteristic of cirrus and
cirrostratus clouds is that these clouds are composed almost
exclusively of ice crystals. Because of the usual scarcity of
freezing nuclei active above -20 degrees C in the atmosphere,
cirrus clouds are not usually found at temperatures higher than
this. Thus, cirrus clouds are usually classed as high clouds.
Cirrus thickness has been statistically shown to have a median

thickness of 1.0 km and has a truncated log normal distribution (11:59).

The LOWTRAN6 program includes a computer subroutine which accounts for cirrus cloud transmittance. In the model, the cirrus cloud transmittance is proportional to the cloud thickness and is independent of wavelength (in the region this report is concerned with). The subroutine default value for cirrus thickness is set at 1 km and the cirrus base altitude is set at 11 km for the tropical model (the default values can be overridden).

Figure 12 is the atmospheric transmittance (including cirrus clouds) as a function of zenith angle from the surface of the earth, and Figure 13 is the atmospheric transmittance as a function of zenith angle from the target (at 10 km).
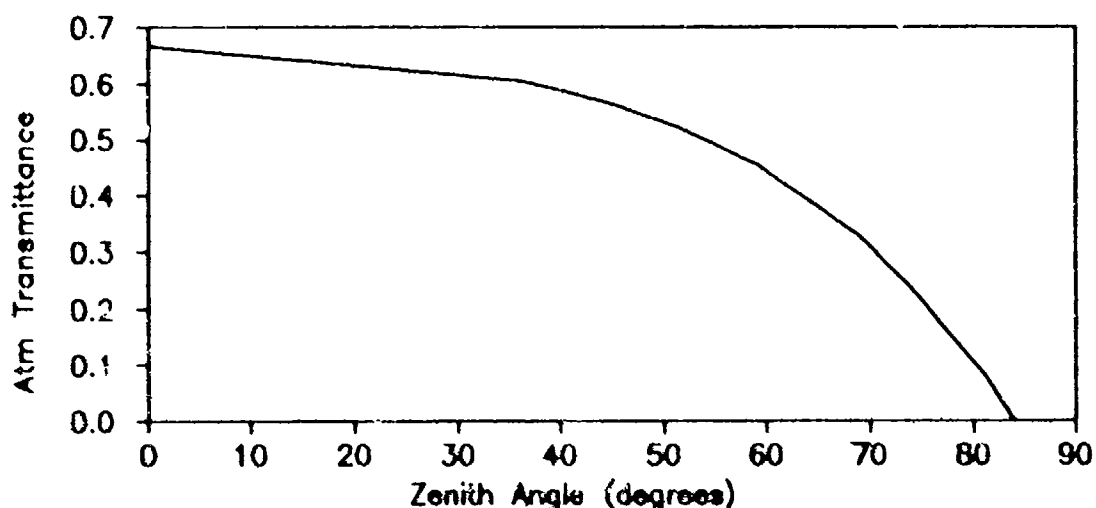
Figure 12. Atmospheric Transmittance (with cirrus clouds) from the earth's surface as a function of zenith angle

33
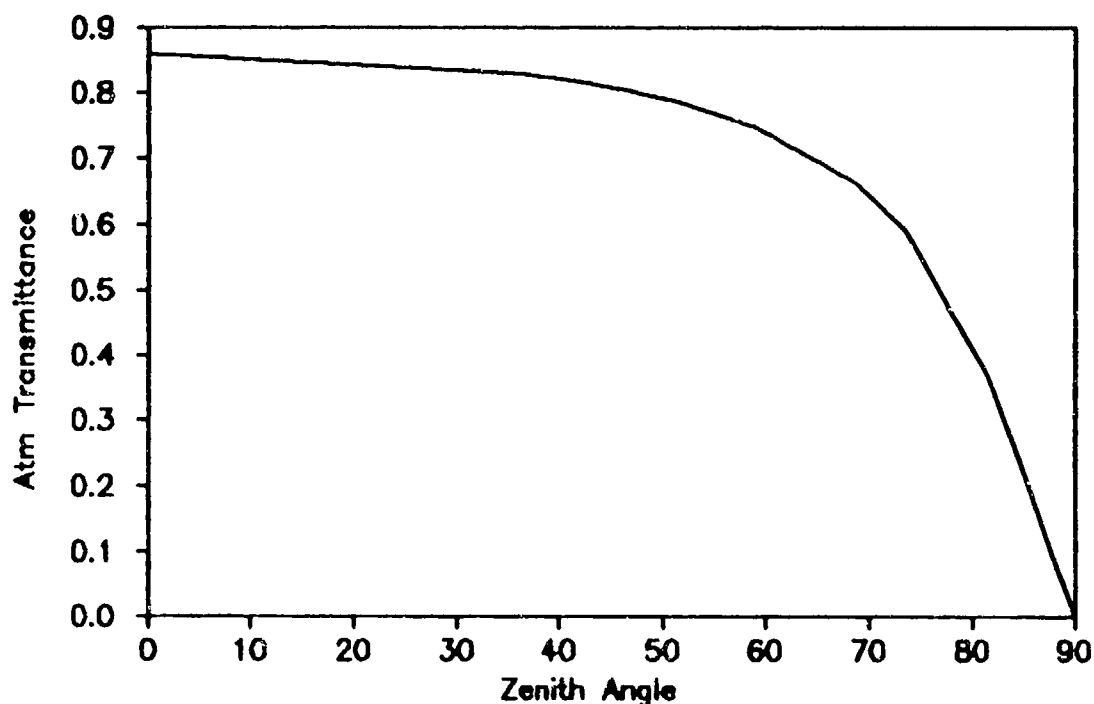
Figure 13. Atmospheric Transmittance (with cirrus clouds) from

10 km as a function of zenith angle

Optimum Operating Wavelength

From Figures 7 and 10, there are certain atmospheric windows which best allow transmission through the atmosphere. The peak emission from the target (from Chapter 4) was 4.25 micrometres. From Figure 10, this wavelength corresponds to a region with very high attenuation caused by the atmosphere.

Peak transmittance through the atmosphere occurs at a wavelength of 3.968 micrometres. Figure 14 illustrates the product of atmospheric transmittance and emission from the target. From

34

Figure 14, the operating wavelength window for 90 % transmission for this system is 3.46 - 4.16 micrometres.
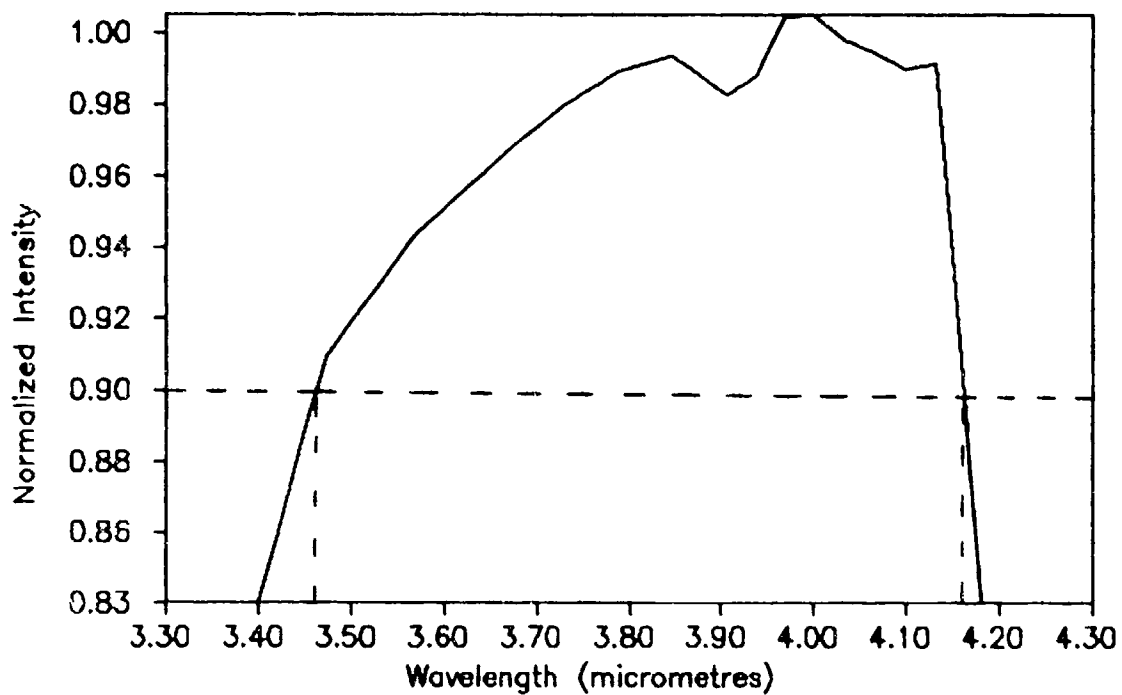
Figure 14. Optimum Operating Wavelength

VI. Satellite Orbital Characteristics

Orbit Shape/Inclination

The purpose of the system being designed in this report is to provide coverage over the area between 120 degrees E and 150 degrees E longitude and 0 degrees to 15 degrees S latitude. As a consequence, the effects of earth rotation on the orbit could be regarded as a disadvantage, rather than the advantage it is to some surveillance systems providing global coverage. The net effect of earth rotation is to displace the ground track of the orbit westward on each successive revolution of the satellite by the number of degrees the earth rotates during one orbital period (1:142). The time required for one complete earth rotation is 23 hours 56 minutes.

In order to negate the effects of earth rotation, a circular equatorial orbit has been selected. A circular orbit does not have an apogee or perigee, so the satellite will be at the same altitude every time it traverses the same point on the earth's surface. With an equatorial orbit, earth rotation does not affect the ground area being flown over, as the ground track is the same.

Number of Satellites

The area to be covered by this satellite system includes 15 degrees in latitude by 30 degrees in longitude. This equates to the area shown in Figure 15.
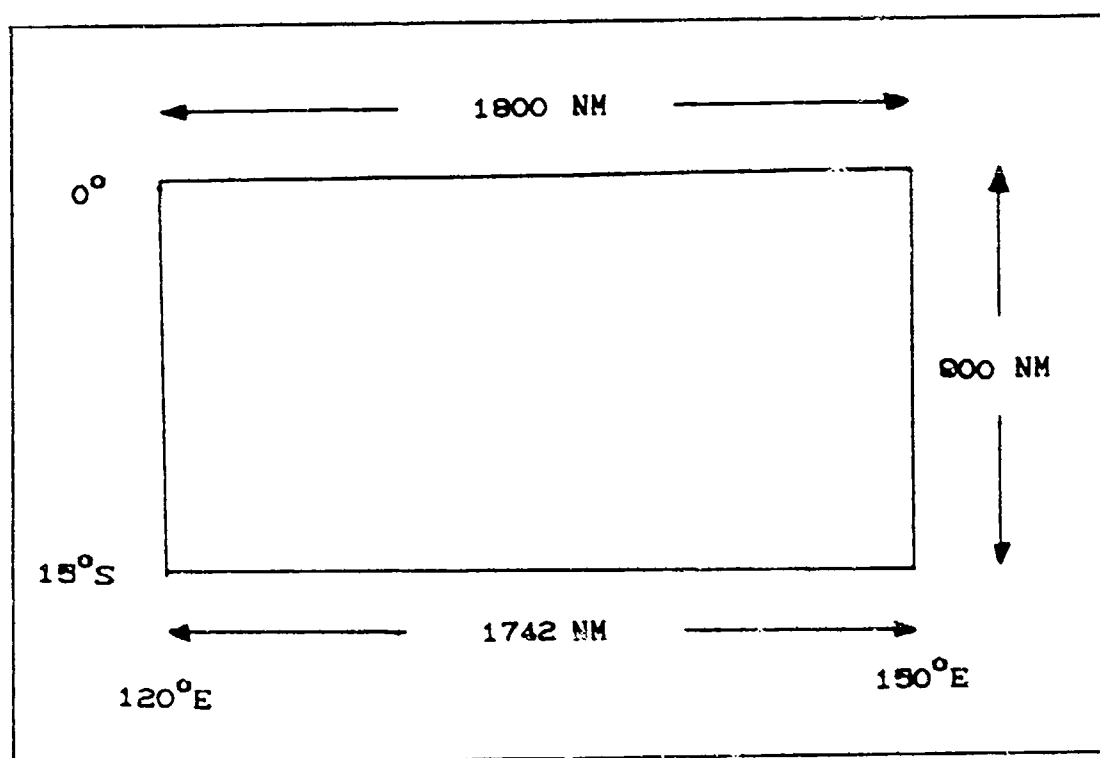
Figure 15. Ground Area Coverage

The size of the ground area observed by a satellite depends on the size of the detector, the focal length of the optics, and the number of detectors that can be placed in the satellite focal plane array. As this information is unavailable at an unclassified level, it has been assumed that one satellite can cover a ground area measuring 900 NM by 900 NM (15 degrees by 15 degrees). (Note: 1 nautical mile (NM) = 1.852 km)

If one satellite can cover 15 degrees in longitude, then the complete constellation will consist of 24 satellites equally spaced, 15 degrees apart in a circular equatorial orbit. This constellation would provide total coverage over the region from the equator to 15 degrees S.

Satellite Altitude

The altitude of the satellite will affect the received irradiance, from both targets and background, and the field of view of each detector (as the ground area to be covered by each satellite has been selected). Figure 16 illustrates that as the altitude (h) is increased, the range (R) increases and the zenith angle (a) through the atmosphere decreases, thereby increasing the atmospheric transmittance.
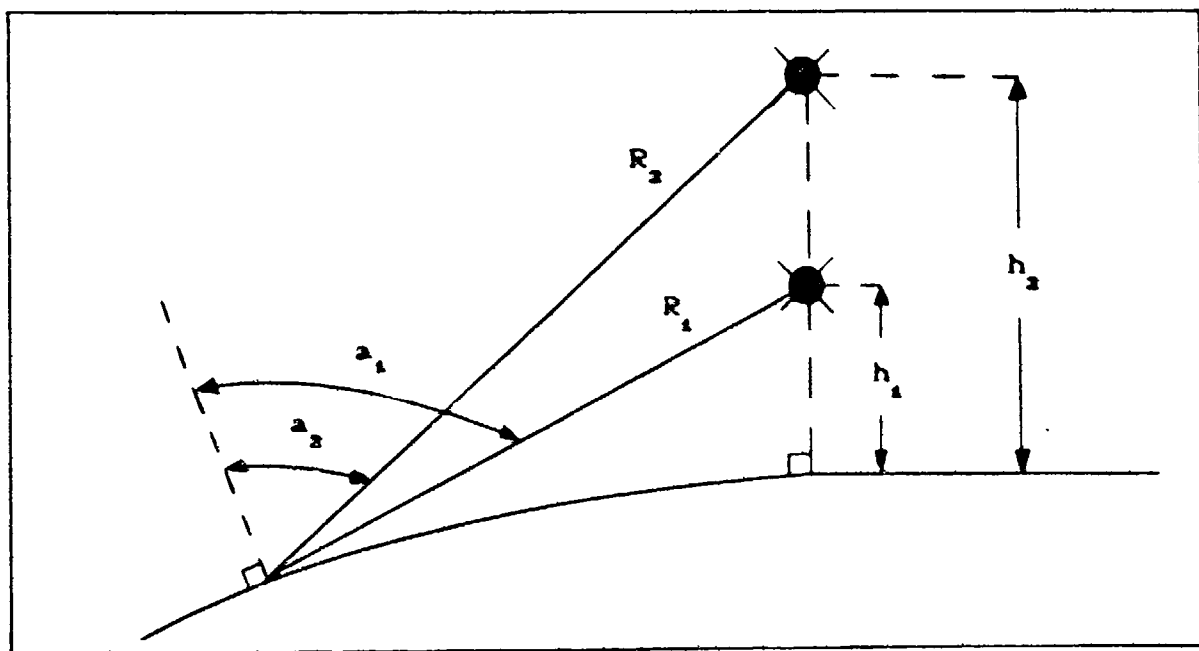
Figure 16. Satellite Altitude, Range and Zenith Angle

38

The following calculations for optimal satellite altitude
are worst case figures and are from the satellite to the farthest
corner of the ground area. That is, from the satellite altitude
above the equator to a point 15 degrees S in latitude and 7.5
degrees E (or W) in longitude from the satellite.

For the background, the received irradiance at the
satellite, assuming a lambertian surface, is

$$E = L \ \Omega(R) \ \tau(a(R)) \qquad (2)$$

where E is the received irradiance $(W \ m^{-2})$

L is the background radiance $(W \ m^{-2} \ ster^{-1})$

Ω is the solid angle of the detector $(ster)$

τ is the atmospheric transmittance

a is the zenith angle

R is the range (m)

The solid angle Ω is approximately equal to

$$\Omega \approx \frac{A}{R^2} \qquad (3)$$

where A is the area on the ground

R is the range from ground to satellite

As the ground area is to be kept constant, irrespective of
altitude, the solid angle is inversely proportional to the range
squared.

39

The data for thermally emitted radiance was derived in Chapter 4, and the atmospheric transmittance figures were derived in Chapter 5. Calculations for deriving the ranges and angles used as a function of altitude are listed in Appendix B.

Figure 17 is a graph of "normalized irradiance" from an extended background as a function of altitude. This graph illustrates that there is an optimal altitude for maximizing irradiance from the surface (or objects close to the surface) and it is a tradeoff between atmospheric transmittance and range. The optimal altitude for peak irradiance from an extended background is approximately 1200 km.

If the irradiance is measured with respect to the target, which has the characteristics of a point source, the received irradiance at the satellite is

$$E = \frac{I \, \tau}{R^2} \qquad (4)$$

where E is the received irradiance $(W \, m^{-2})$

    I is the target intensity $(W \, ster^{-1})$

    τ is the atmospheric transmittance

    R is the range (m)
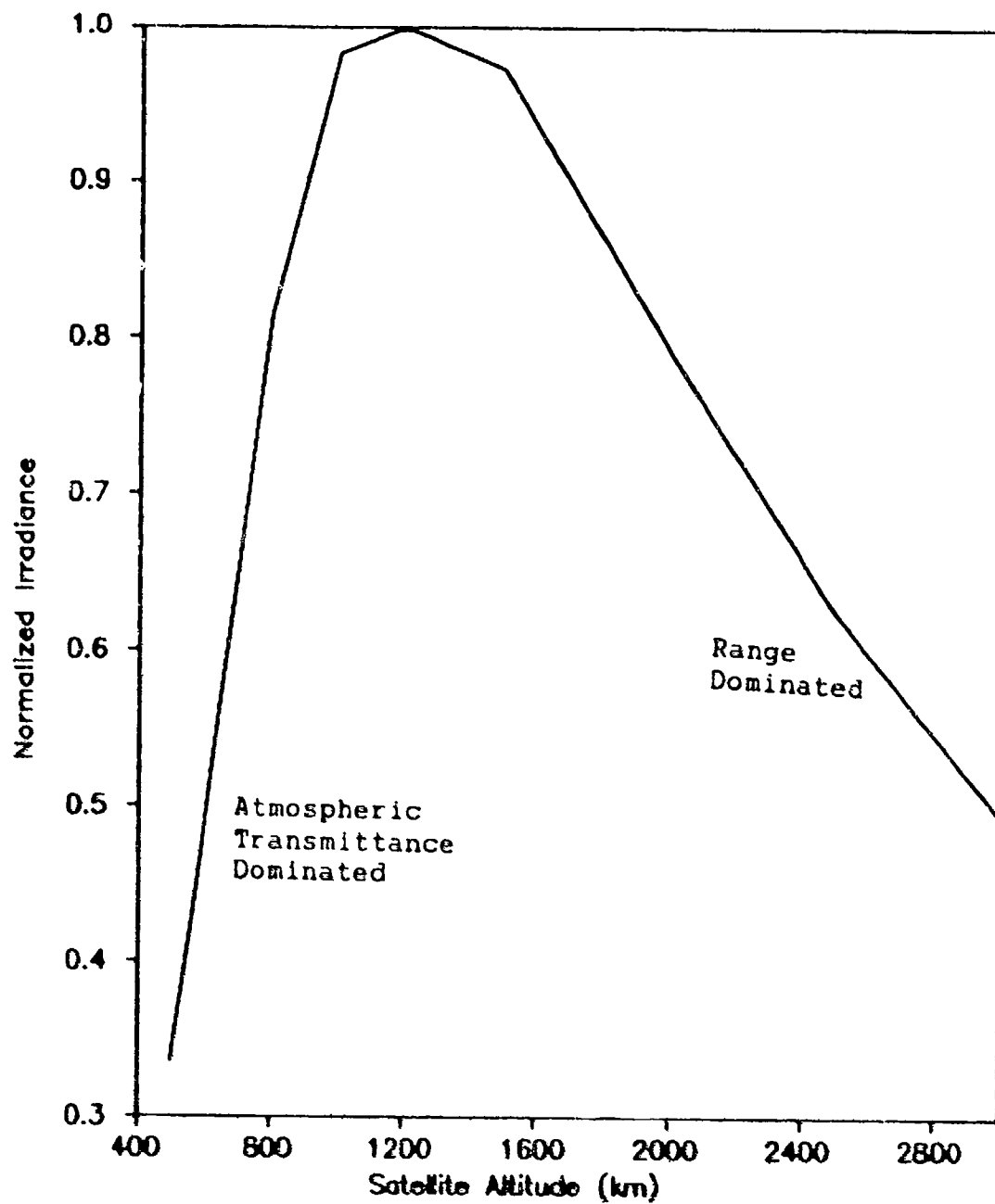
Figure 17. Optimum Satellite Altitude for Background

41

Since the target is at an altitude of approximately 10 km, the atmospheric transmittance will be different from that for a object closer to the earth's surface (their ranges will approximately be the same). Figure 18 is a plot of the "normalized irradiance" from the target as a function of altitude. The optimal satellite altitude for peak irradiance from a target at 10 km is approximately 400 km.

Figures 17 and 18 show that the optimal satellite altitude is different for an object at a height of 10 km as that from an object or extended source at the earth's surface. The satellite optimal altitude is very dependent on the height of the infrared source, as the atmospheric attenuation is greater in the lower levels of the atmosphere.

If the target was guaranteed to be flying at an altitude of 10 km, the optimal satellite altitude would be approximately 400 km and the atmospheric transmittance from the target would be much greater than the atmospheric transmittance from the earths background. Whether a target can be detected (the amount of received irradiance) is more important than the relative amounts from background and target as the background will be eliminated by the signal processing (background limited). Background limited will be discussed in Chapter 6.
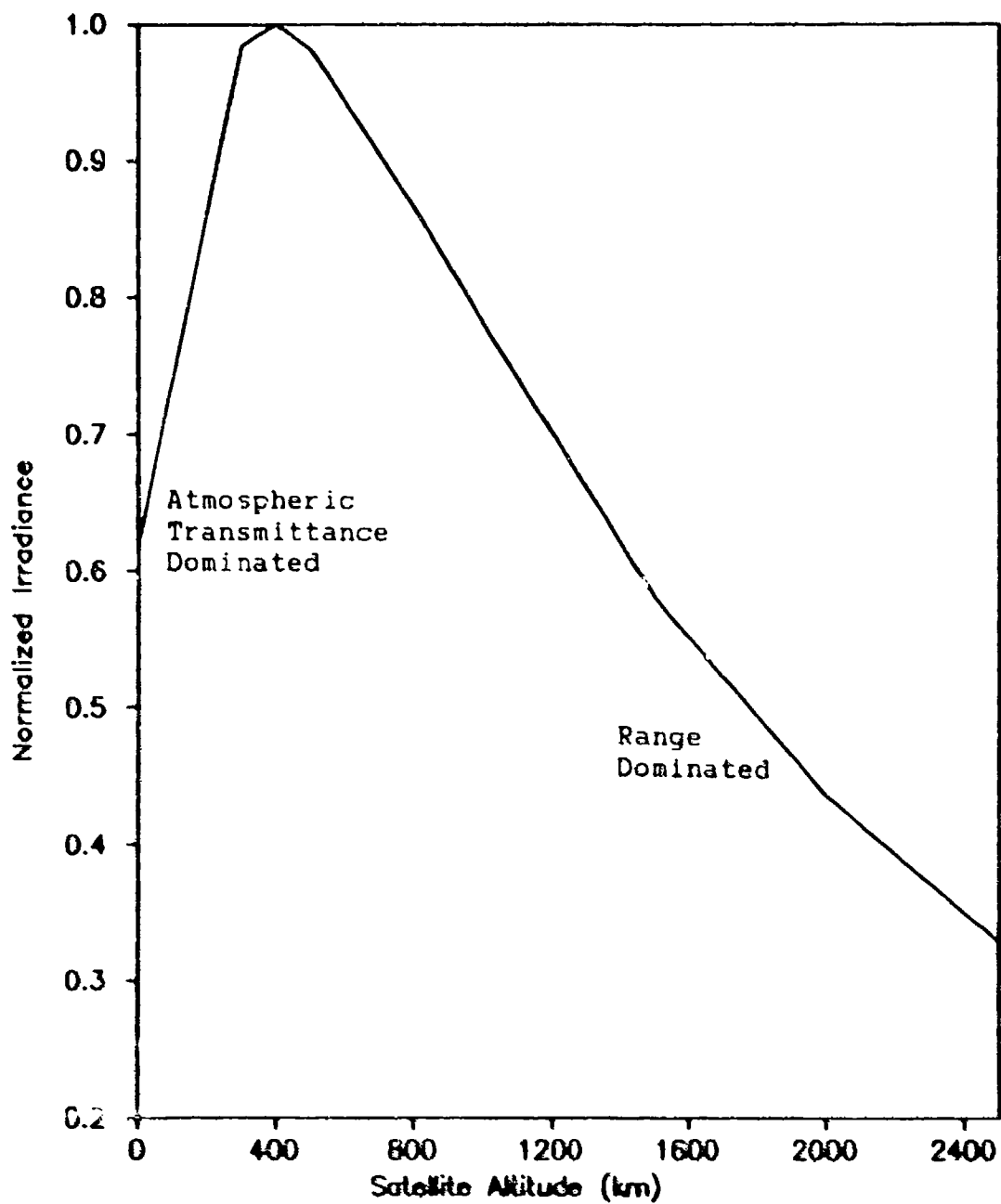
Figure 18. Optimum Satellite Altitude for Target (@ 10 km)

As the aircraft could be flying at a lower altitude, a higher satellite altitude would appear to be preferential. As the aircraft's altitude is decreased, the optimal satellite altitude will increase as the atmospheric attenuation will increase for higher zenith angles from the target's new location.

Another factor that would have to be considered in selecting the satellite altitude is the focal length of the satellite optics. The ratio of the effective focal length (f) to the detectors active image size (d) is equal to the ratio of the range to the target (R) to the size of the ground resolution cell(L), where $L = \sqrt{A}$.

$$\frac{f}{d} = \frac{R}{L} \qquad\qquad (5)$$

As the detector image size and the ground resolution cell size is constant, the focal length is proportional to the range to the target (satellite optics will be discussed in more detail in the next chapter).

Irradiance across the image plane of the detector is not uniform, as there is at least a cosine squared dropoff of focal plane irradiance as you move further away from the normal (refer Figure 19).

44
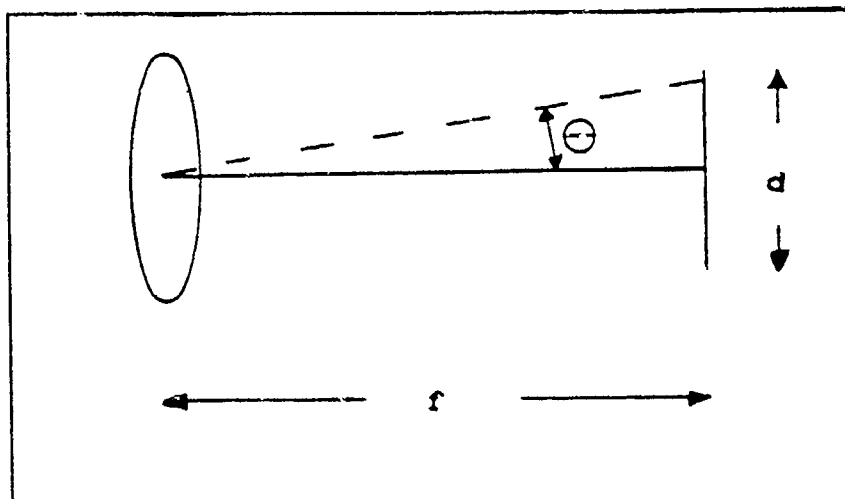
Figure 19. Focal Plane Irradiance

As the lens is moved further away from the focal plane
(increasing the focal length), all the points on the focal plane
approach the same distance away from the lens. Therefore, more
uniform focal plane irradiance can be obtained with a larger
focal length.

Table 2 illustrates the improvement in focal length with
altitude that can be obtained compared with a satellite located
at an altitude of 400 km. The focal length improvement factor is
defined as

$$f_{imp} = \frac{f_{Alt} - f_{400}}{f_{400}} \times 100\% \qquad (6)$$

Other information provided is the ratio of irradiance received from the target compared to peak target irradiance (for an altitude of 400 km), and irradiance received from background compared to peak background irradiance (for an altitude of 1200 km).

Table 2. Focal Length Improvement versus Altitude

Altitude	Range	% E (target)	% f improve
400	1762	100	—
600	1842	95	4.5
800	1939	86	10.0
1000	2051	78	16.4
1200	2176	68	23.5
1400	2311	60	31.2
1600	2455	53	39.3

As the selection of satellite altitude depends on a 'best fit' between received irradiance and optics focal length, system and component specifications would have to be considered for final selection. As actual specifications are not being used in this design, selection of a satellite altitude is arbitrary.

There is a 16 % improvement in the optics focal length for an change in satellite altitude from 400 km to 1000 km while the

amount of irradiance received from the target has only decreased
by approximately 22 %. Therefore, a satellite altitude of 1000 km
has been selected for this system.

Satellite Speed

The period of a circular orbit is given by (1:33):

$$TP = \frac{2\pi \ r^{3/2}}{\mu^{1/2}} \tag{7}$$

where TP is the total period

r is the radius (earths radius + altitude)

μ is the gravitational parameter
$(3.986 \times 10^5 \ km^3/sec^2)$

For h = 1000 km, the total period is 105.1 minutes. This
equates to 3.43 degrees/min, so the satellite is moving
relatively slowly across the earth's surface (at a speed of 3.43
NM/sec or 6.35 km/sec).

As the satellite will be operating in a step-staring mode,
the speed of the satellite relative to the earth's surface is
important to determine suitable step sizes which would be within
the capabilities of the satellite hardware. As the speed of the

47

satellite relative to the earth's surface is not high, step-
staring of the satellite sensor would not be a problem.

VII. Satellite Focal Plane Array

As outlined in Chapter 2, the Charge Coupled Device allows a high rate of data to be extracted from a focal plane array. General information on CCD operation and expected performance was also discussed in Chapter 2. Letters were sent to CCD manufacturers requesting information on current capabilities of Infrared CCDs but little useful information was provided (probably due to the classified nature of the material).

Eastman Kodak is currently developing Infrared CCDs for remote sensing. As an example of their current capabilities in the visible wavelength region, they have a CCD imager that has 1,336,200 pixels in its focal plane array, with each pixel having an active image area of 6.8 micrometres x 6.8 micrometres (10:1). These figures will be used as a guideline for selecting figures to be used for this system.

A size of 4 square centimetres has been arbitrarily selected for the focal plane array, as this appears a realistic figure in terms of physical size. If a pixel active image size of $d = 20$ micrometres square is selected, one could safely assume that an actual infrared detector pixel would be smaller in size. This implies that, for this system, the number of pixels would be 1000 x 1000 or 1 million (refer Figure 20).
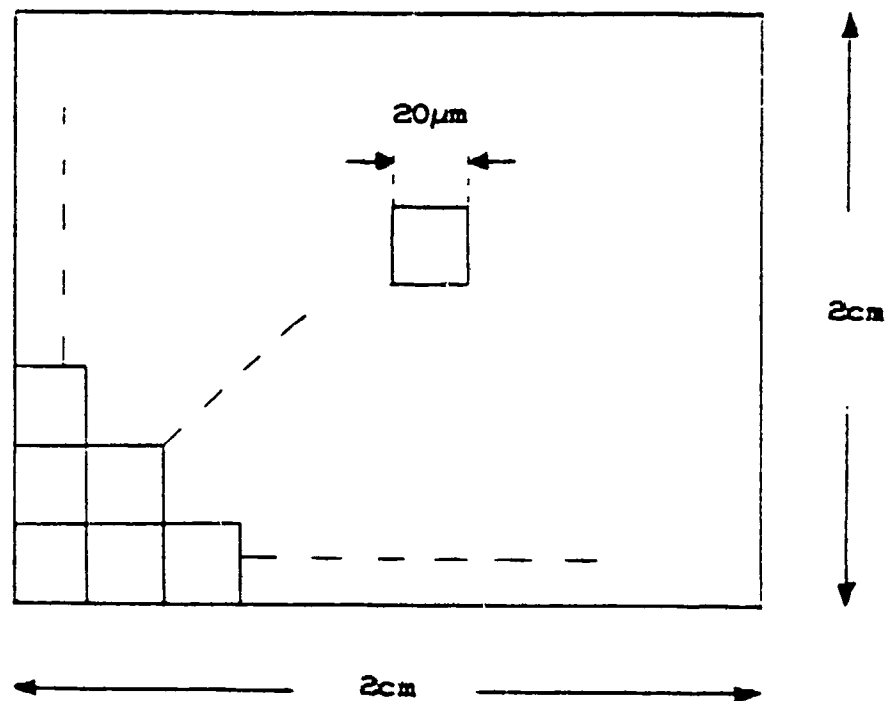
Figure 20. Focal Plane Pixel Layout

When this pixel size is transferred to the size of the resolution cell covered on the earth, one finds the size covered by each pixel is

L = (900 NM x 1.852 km/NM)/1000 pixels = 1.67 km

Satellite Optics

As discussed in the previous chapter, satellite altitude (or more precisely, distance from satellite to target) affects the selection of the optics used in the satellite. Figure 21 illustrates the relationship between the lens focal length,
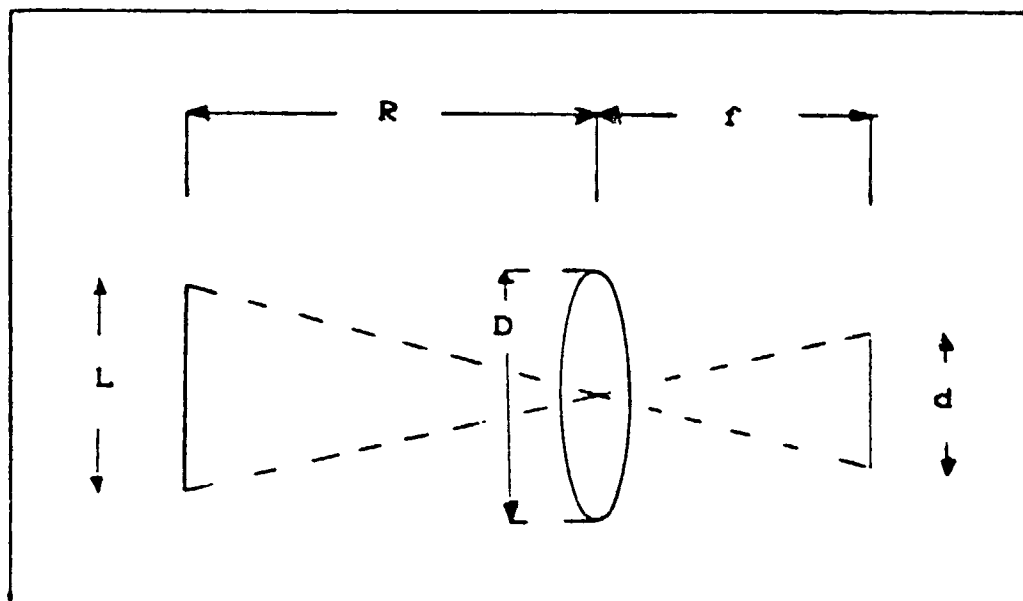
Figure 21. Satellite Optics

range, pixel image size and ground resolution cell size, with the relationships between these elements being expressed in Equation (5) on page 44.

For a range of 2051 km (altitude of 1000 km), a pixel image size of 20 micrometres and a ground resolution cell size of 1.67 km, the effective focal length required is f = 2.46 cm.

Diffraction is the ultimate limit to the spatial resolution of an optical system and arises from the wave nature of light. Broadly speaking, it means a point source of light cannot be

focused down to a point by the optics system, but will appear as an Airy pattern. The Airy pattern consists of a circular area of light (Airy disk) surrounded by rings of rapidly decreasing intensity (21:8-27). The Airy disk contains 84% of the power entering the optics from a point source, and the diameter of the Airy disk (S) is dependent on the diameter of the collecting optics (D), the focal length (f) and the wavelength of the light (14:138).

$$S = 2.44 \frac{f \lambda}{D} \tag{8}$$

The size of the Airy disk would have to be less than the size of the detector pixel. As illustrated in Figure 22, if the size of the Airy disk was about the same size as the detector pixel, the Airy disk would overlap as many as four separate pixels. This would not allow for accurate positioning of the target, so a smaller Airy disk (or a larger pixel) would be required. If the Airy disk was much smaller than the detector pixel, the Airy disk would be more likely to be in a single pixel.

The probability of the Airy disk being completely within one pixel can be calculated. Referring to Figure 23, anytime the centre of an Airy disk of diameter S is greater than the radius of the disk away from the edge of the pixel of size d, there will be no overlapping with neighboring pixels (assuming no gap

Aircraft Flight Direction
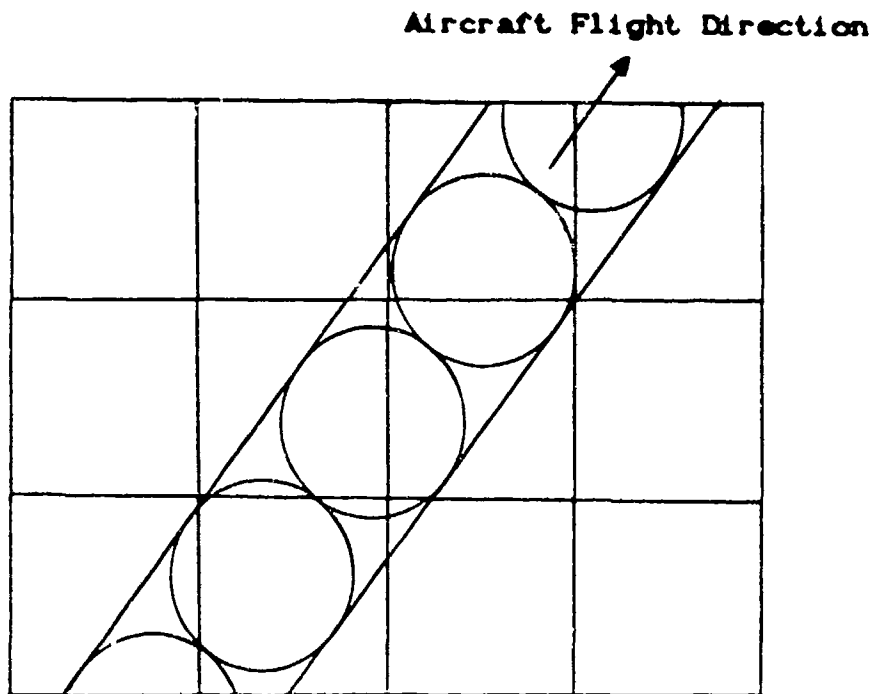
Figure 22. Airy Disk Size
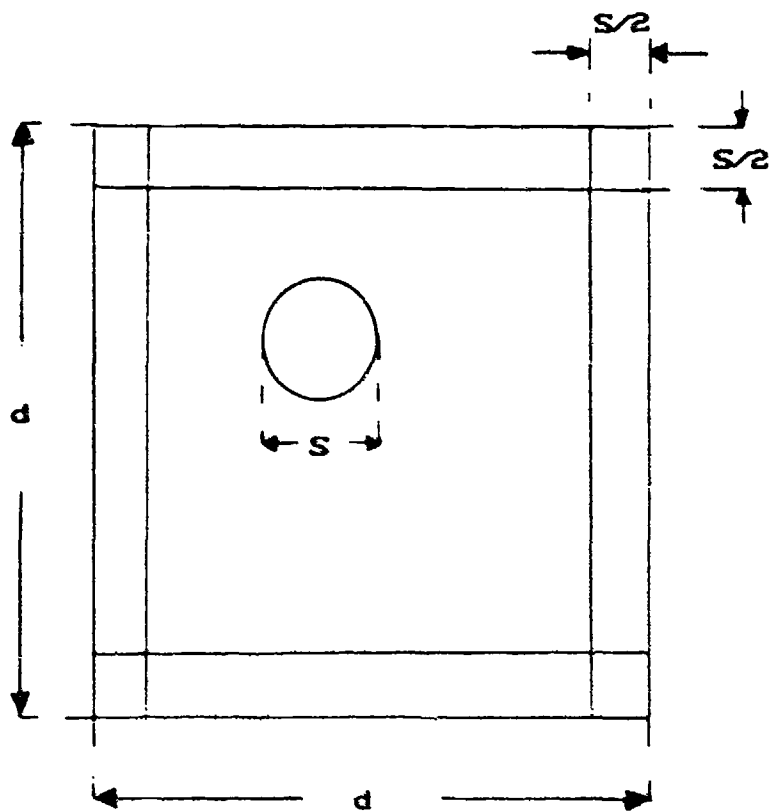
Figure 23. Airy Disk Probability Chart

between pixels). From simple geometry, the probability of the
Airy disk being completely within one pixel is

$$P(1) = \frac{(d-s)^2}{d^2}$$

(8)

For S = 0.10 d , P(1) = 0.81

S = 0.05 d , P(1) = 0.9025

S = 0.01 d , P(1) = 0.9801

The tradeoff for increasing the probability of the Airy disk
being within one pixel is an increase in the size of the
collecting optics. While increasing the size of the optics will
increase the amount of power (number of photons) received, the
size must be kept within the limits suitable for satellite use.
Therefore, an Airy disk size (S) of 0.05 d has been selected.
This gives a probability of the Airy disk being entirely within
one pixel of 90 %. The size of the collecting optics (D) will be,
from Equation 8:

$$D = \frac{(2.44)\ (2.46 \times 10^{-2})\ (4 \times 10^{-6})}{(0.05)\ (20 \times 10^{-6})}$$

$$= 24\ cm$$

Scanning Method

Chapter 4 discussed detection requirements for the system and gave values for the time taken for an aircraft to traverse various resolution cell sizes. For a resolution cell size of 1.67 km, an aircraft would traverse the resolution cell in 6.5 seconds.

Integration time is the time the detector is 'looking' at a scene and collecting photons before this information is fed to the data processing system. The maximum integration time occurs when the detector receives enough photons to saturate the detector material. The procedure for calculating the maximum integration time will be described in the next chapter. For the purposes of this system, one can assume (based on manufacturers' figures on actual detectors) that the integration time is very much less than 1 second.

As the maximum integration time per detector is less than one second and the aircraft takes 6.5 seconds to fly completely across the resolution cell, the detector could collect at least ten individual responses from the target with respect to the one resolution cell. This would appear to be more information than was needed, and would not be necessary for accurate positioning of the target. As discussed in Chapter 4, two successful detections within each resolution cell would appear reasonable

and would result in a maximum time between detections of less than 5 seconds.

If a focal plane array detector pattern, as illustrated in Figure 24, was used, the satellite could step-stare across the scene, with the rows of detectors staring at a row of ground resolution cells for the integration time of the detectors, then moving on to the next row of resolution cells. If an aircraft was flying all the way through a resolution cell, one would get at least two responses from the target for that individual resolution cell.
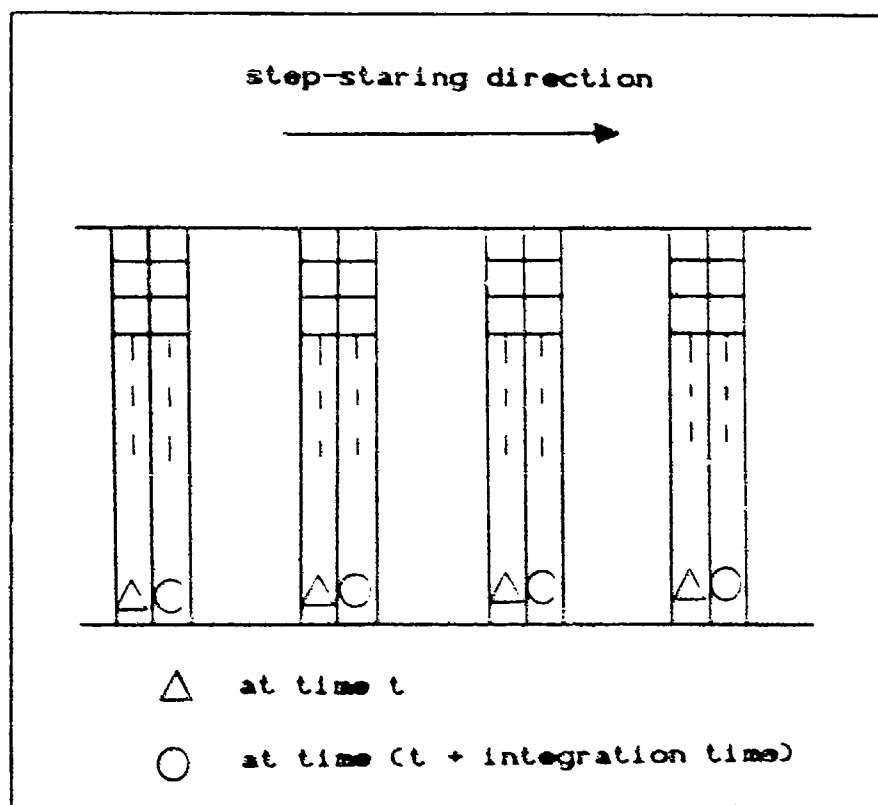
Figure 24. Focal Plane Array Detector Pattern

The advantage of this focal plane array is that there are fewer detectors than a full staring sensor, which would mean cheaper cost. Also, with fewer detectors, there would be less data for the data processing network to handle. If a single detector in the array was not working, this would not be a serious problem as other detectors would be scanning across the resolution cell and targets would still be detected.

VIII. System Calculations

This chapter will present the various information that would be required to calculate the actual received irradiance at the satellite, as well as the power throughput to the detector. As most of the information required to perform these calculations is unavailable, the equations have been presented; and for an actual system design, the required numbers can be inserted and system requirements can be calculated.

Noise Analysis

The following CCD noise analysis is taken from Dereniak and Crowe (6:237). There are a number of noise sources that limit the sensitivity of a system using a CCD focal plane. There are noises associated with the scene photon flux, noises related to the CCD itself, and noises related to the output preamplifier. These noise sources are illustrated in Figure 25. A list of the various noise sources is given in Table 3. As the independent sources of noise add in quadrature, to obtain the total noise one must root sum square all the noise sources. Further information and equations for calculating the noise currents is included in Dereniak and Crowe (6:241).
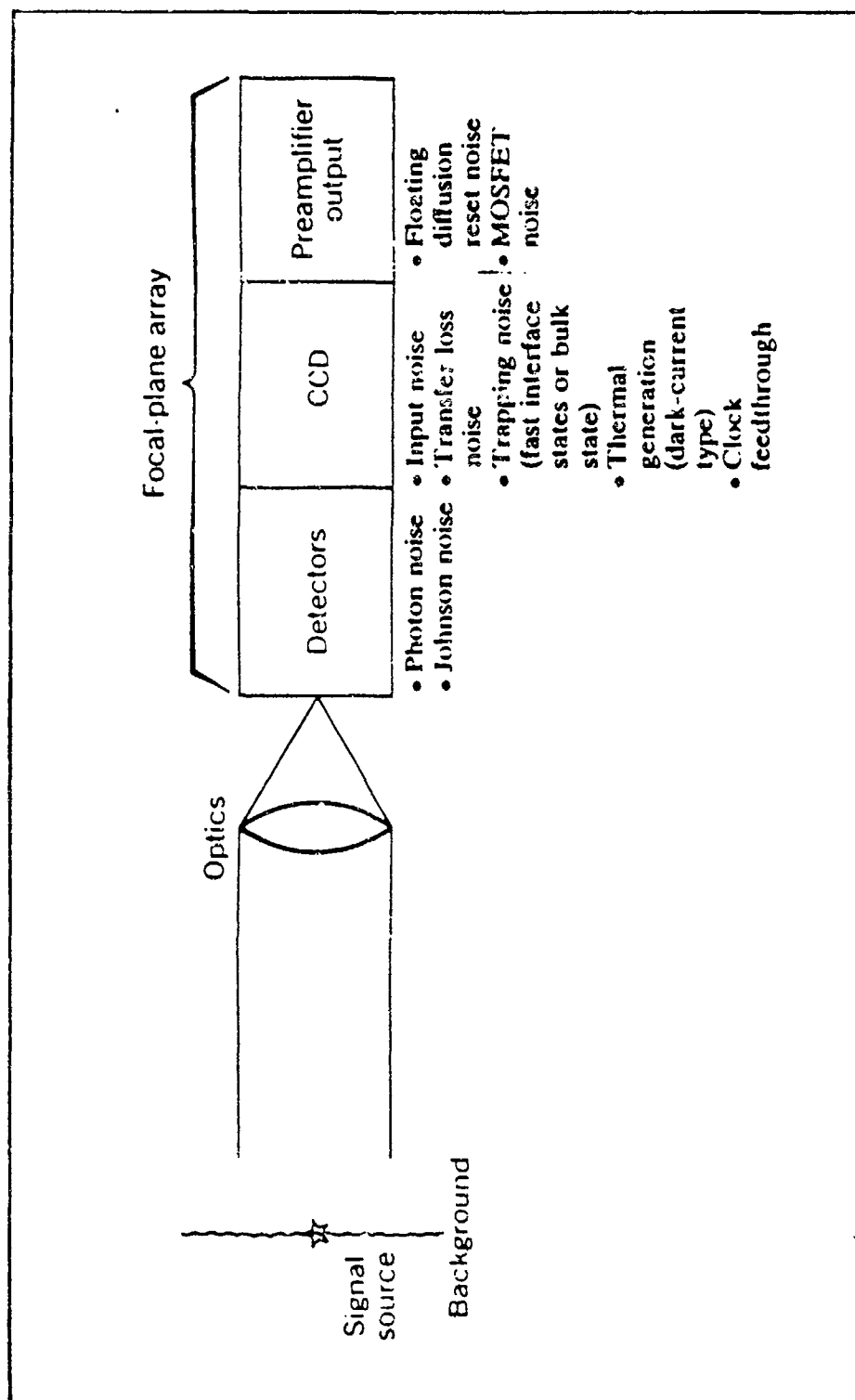
Figure 25. CCD Noise Sources

Table 3.   Types of Noise in CCD Focal Plane Array (6:238)

Noise Type	Description
Photon Noise	This manifests itself as shot noise due to the random arrival and emission rates of photons.
Input Noise	Random injection of charge from a diffusion into a potential well.
Transfer Inefficiency Noise	The noise associated with with the random amount of charge lost by a signal upon tranfer and the amount of charge introduced to a signal upon entering a well.
Trapping Noise	A noise arising from random trapping emission from interface states.
Dark-current Noise	This noise is associated with carriers that are thermally generated to bring the potential well into thermal equilibrium.
Clock Feedthrough Noise	This noise is due to capacitance coupling from the array gates to the output diode.
Floating Diffusion Reset Noise	This is noise associated with the reset circuit on the output preamplifier.
Amplifier Noise	This noise is associated with a MOSFET of a given transconductance.
Detector Uniformity Noise	This noise is variations across the video output for a uniform radiation flux input.
Read Noise	Noise associated with reading the information from the focal plane array - independent of time between reads.

Integration Time

As mentioned in the previous chapter, the maximum integration time occurs when the detector receives enough photons to saturate the detector material. The number of photons required to saturate the detector can be calculated from the specifications for the detector and varies with detector material and size.

The following derivation of maximum integration time is taken from Lange and Evans (14:218).

$$
\begin{bmatrix} \text{Number of} \\ \text{photons to} \\ \text{saturate} \end{bmatrix} = \begin{bmatrix} \text{Power} \\ \text{Received} \end{bmatrix} \begin{bmatrix} \text{Maximum} \\ \text{Integration} \\ \text{Time} \end{bmatrix} \bigg/ \begin{bmatrix} \text{Energy per} \\ \text{Photon} \end{bmatrix}
$$

$$
\begin{bmatrix} \text{Power} \\ \text{Received} \end{bmatrix} = \begin{bmatrix} \text{Irradiance} \\ \text{on} \\ \text{Satellite} \end{bmatrix} \begin{bmatrix} \text{Collecting} \\ \text{Optics} \\ \text{Area} \end{bmatrix} \begin{bmatrix} \text{Optics} \\ \text{Transmission} \\ \text{Factor} \end{bmatrix}
$$

$$
\begin{bmatrix} \text{Maximum} \\ \text{Integration} \\ \text{Time} \end{bmatrix} = \frac{\begin{bmatrix} \text{Number of} \\ \text{Photons to} \\ \text{Saturate} \end{bmatrix} \begin{bmatrix} \text{Energy per} \\ \text{Photon} \end{bmatrix}}{\begin{bmatrix} \text{Irradiance} \\ \text{on} \\ \text{Satellite} \end{bmatrix} \begin{bmatrix} \text{Collecting} \\ \text{Optics} \\ \text{Area} \end{bmatrix} \begin{bmatrix} \text{Optics} \\ \text{Transmission} \\ \text{Factor} \end{bmatrix}} \quad (10)
$$

Received Detector Currents

The received detector current will consist of two components, one from the target and one from the background. As the target is a point source and the background is an extended source, two different equations are required to calculate the two quantities. These calculations would be performed for each detector.

For the target, this equation is from Lange and Evans (14:219), where it is assumed that the target is near the centre of the field of view.

$$i_t = e \int_{\lambda_1}^{\lambda_2} \eta(\lambda) \; G \; \frac{I_\lambda(\lambda) \; \tau_{atm}^{tar}(\lambda) \; \lambda}{R^2 \; h \; c} \; \tau_{opt}(\lambda) \; A_2 \; d\lambda \tag{11}$$

where i_t = current from target (amps)

            e = 1.6×10^{-19} coulombs

            η = quantum efficiency (electrons/photon)

            G = detector Gain

            I_λ = spectral intensity of target $(W \; ster^{-1} \; \mu m^{-1})$

            τ_{atm}^{tar} = atmospheric transmittance for target

            λ = wavelength (μm)

$$h \quad = 6.626 \times 10^{-34} \; J.s$$

$$c \quad = 3 \times 10^{14} \; \mu m/s$$

$$A_R \quad = \text{collecting optics area} \; (m^2)$$

$$\tau_{opt} \quad = \text{optics transmission factor}$$

$$\lambda_1 \rightarrow \lambda_2 \quad \text{is the bandpass of the detector} \; (\mu m)$$

$$R \quad = \text{range} \; (m)$$

For the background, the equation is (14:222), assuming L_λ is uniform across Ω

$$i_b = e \int_{\lambda_1}^{\lambda_2} \eta(\lambda) \; G \; \frac{L_\lambda(\lambda) \; \Omega_R \; \tau_{atm}^{bac}(\lambda) \; \lambda}{h \; c} \; A_R \; \tau_{opt}(\lambda) \; d\lambda \qquad (12)$$

where $i_b \quad = \text{current from background} \; (amps)$

$L_\lambda \quad = \text{spectral radiance of the background}$
$(W \; m^{-2} \; ster^{-1} \; \mu m^{-1})$

$\Omega_R \quad = \text{field of view of the detector} \; (ster)$

$\tau_{atm}^{bac} \quad = \text{atmospheric transmittance for background}$

Signal to Noise Calculations

The signal to noise ratio is defined as

$$\frac{S}{N} = \frac{i_{signal}}{i_{noise}} = \frac{i_{signal} \Big/ e}{i_{noise} \Big/ e} \qquad (13)$$

One normally requires a S/N ratio greater than three in order to detect the signal, with the actual value being dependent on the detector. While i_{signal} is the current received from the target, i_{noise} results from all current sources including the background current.

The signal to noise ratio is then

$$\frac{S}{N} = \frac{i_{signal}}{\left[i^2_{background} + i^2_{thermal} + i^2_{shot} + \dots - (\bar{i})^2 \right]^{1/2}} \quad (14)$$

where $i_{thermal}$, i_{shot} etc are noise sources and
$\bar{i}$ is the average noise value.

Even though the background current is often very large, it can almost always be subtracted out as it is reasonably constant over the integration time (13:12A). If the system is background limited, the background is much larger than any other source (the ratio of background current to signal current will be calculated in the next section). Assuming the system is background limited, then $\bar{i} \approx i_{background}$ and the signal to noise ratio is

$$\frac{S}{N} = \frac{i_{signal}}{\left[i^2_{thermal} + i^2_{shot} + --- \right]^{1/2}} \qquad (15)$$

Shot noise is due to the random arrival and emission rate of photons, and is often the dominant noise source.

$$i_{shot} = \left[\frac{e\ \bar{i}}{t_d} \right]^{1/2} \qquad (16)$$

where $e = 1.6 \times 10^{-19}$ coulombs

t_d = integration time

Assuming shot noise is dominant, in the background limited mode :

$$\frac{S}{N} = \frac{i_{signal}}{\left[\frac{e}{t_d}\ i_{background} \right]^{1/2}} \qquad (17)$$

Ratio of Signal to Background Current

From equations (11) and (12), and assuming I_λ and L_λ are approximately constant over the system bandpass,

65

$$\frac{i_t}{i_b} = \frac{I \; \tau_{atm}^{tar}}{R^2 \; \Omega_R \; L \; \tau_{atm}^{bac}}$$
(18)

$$\text{As } \Omega_R \approx \frac{\text{Ground Resolution Cell Area (A)}}{R^2}$$
(19)

$$\frac{i_t}{i_b} = \frac{I \; \tau_{atm}^{tar}}{A \; L \; \tau_{atm}^{bac}}$$
(20)

Using values from chapters 4, 5, 6, and 7

$I \approx 900$ W/Ster

$L \approx 0.785$ W/m^2.Ster

$A \approx (1.67 \times 10^3)^2$ m^2

$\tau_{atm}^{tar} \approx 0.9725$

$\tau_{atm}^{bac} \approx 0.4850$

$$\frac{i_t}{i_b} = 8.25 \times 10^{-4}$$

From the above calculation, this system is definitely background limited, as assumed earlier.

The signal to noise ratio for the proposed system can be

estimated using the above values as well as the following values
and assumptions.

Assumptions	Proposed system Values
$\eta = 0.1$	$D = 24$ cm
$G = 1.0$	$A_R = \pi \, (.12)^2$
$\tau_{opt} = 0.5$	$R = 1000$ km
$t_d = 10^{-9}$ s	$\Delta\lambda = 4.16 - 3.46 \; \mu m$
	$= 0.7 \; \mu m$
	$\bar{\lambda} = 4.0 \; \mu m$

Assuming constant I_λ and L_λ, from equation (11)

$$i_t \approx 4.46 \times 10^{-12} \text{ amps}$$

From equation (12)

$$i_b \approx 5.40S \times 10^{-9} \text{ amps}$$

From equation (17)

$$\frac{S}{N} \approx 4.794 = 6.8 \text{ dB}$$

As this figure is greater than 3, this proposed system would
would be able to detect the presence of a target.

IX. Life Cycle Cost Methodology

This chapter outlines the methodology which would be followed
in order to calculate life cycle costs (LCC) for the system.   A
primary function of the long range planning process for a system
is to identify alternatives which are preferential to others
and that satisfy system requirements. Cost Analysis deals with
the problem of determining the resource impact of the
alternative proposals. Estimating the resource requirements of
future systems involves a great deal of uncertainty, and the
following methodology outlines the procedure involved to
calculate the life cycle costs of alternatives.

LCC Methodology

The first phase of the methodology involves time phasing the
system. Referring to Figure 26, the various system costs must be
estimated for each year of the system life. For most years, a lot of
the component costs will be zero, and which component costs are
zero will change as time moves forward.
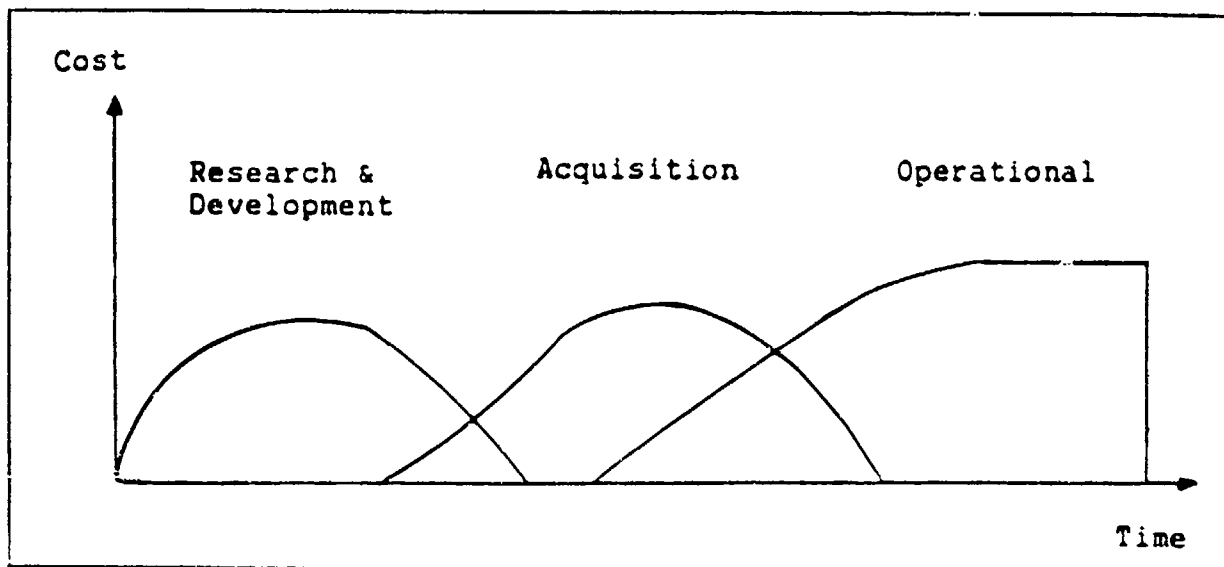
Figure 26. Time Phasing of LCC Costs

Let a_{11} = cost of component 1 in year 1

a_{21} = cost of component 2 in year 1

a_{12} = cost of component 1 in year 2

:

:

a_{N1} = cost of component N in year 1

a_{NM} = cost of component N in year M

The component cost can be one of two types of values :

1. a_{ji} is a known value (a constant), or

2. a_{ji} is a random variable.

If a_{ji} is a random variable, it can be derived from a cost estimating relationship or it can be a random drawing from a probability density function. The main probability distributions

69

used are the Beta and Triangular distributions, where a low and high cost estimate are used as well as a most likely estimate.

For each year, the component cost must be summed :

$$C_1 = \sum_{j=1}^{N} a_{j1}$$

$$C_2 = \sum_{j=1}^{N} a_{j2}$$

$$\vdots$$

C_1 is the total estimated cost in year 1, and C_2 is the total estimated cost in year 2, etc .

The Life Cycle Cost of the system is

$$LCC = \sum_{\iota=1}^{M} \frac{C_\iota}{(1+r)^\iota} \qquad (21)$$

where r is the discount rate $(r > 0)$, with the cost analyst determining its actual value.

As a result, each C_j is a sum of random variables, as is the Life Cycle Cost. Therefore, in order to generate useful statistics, the random number generation must be completed 500 - 1000 times. From the results of the multiple generations, confidence intervals can be expressed about the Life Cycle Costs.

70

X. Conclusions

The purpose of this report has been to describe the methodology that would be involved in designing a system to detect aircraft against a background of the earth. For the purposes of the report, an area on the earth's surface from 0 degrees to 15 degrees S latitude and 120 degrees to 150 degrees E longitude was selected as the region over which detection was required. Also, a target aircraft was selected, and this aircraft is a suitable aircraft with respect to the probable military mission of the detection system. The reason it was selected is that it was the only aircraft that information was found on at an unclassified level.

The major problem which has occurred in completing this report has been the lack of suitable unclassified data. This has resulted in numerous assumptions being made, with these assumptions being best estimates, or designed so that an actual operational system would perform better (i.e. worst case figures). Consequently, these assumptions might not have led to the development of the optimal system.

The methodology has been divided into separate chapters, with the following areas having been covered:

1. Target Detection Requirements

2. Atmospheric Absorption

3. Satellite Orbital Characteristics

4. Satellite Focal Plane Array and Optic

5. System Calculations

6. Life Cycle Cost Methodology

The methodology contained in this report would be similar for most systems that are designed for detection of an aircraft against a background of the earth. One can either work from target through to detector and specify a requirement for a detector, or have a detector and work back to specify the minimum target intensity that can be detected.

It cannot be accurately predicted if a system as proposed in this report can be implemented, as calculations with actual figures have not been completed. If the Teal Ruby experiment is used as a comparison, the technology for detecting aircraft against a background of the earth appears feasible.

This system is based upon a detector operating with Charge Coupled Devices (CCD's), which is the same principle used in Teal Ruby. The CCD appears the optimal type of detector for a staring sensor due to the high amount of data that has to be read from the focal plane array. The amount of data that has to be read from the focal plane array for this system has been reduced by decreasing the number of detectors. This was a tradeoff against

72

the time between detections and would be decided, in an operational system, based on required detection specifications.

Follow On Research

Any further research that could be performed in this area would have to be completed at a classified level. This would allow actual data to be used, and would therefore produce meaningful results that could be directl used for comparisons as to whether the development of a system is feasible.

One area that could be developed further in the future would be the focal plane array. Ti is a tradeoff between data processing limitations, time between detections, and the number of detectors, and this tradeoff could be directly applied to a specific system requirement. Another possible research area would be analyzing possible methods to reduce the number of satellites in the constellation, as 24 satellites appears to be too many.

Appendix A. LOWTRAN 6 Input Instructions

The following is a list of instructions for using the
LOWTRAN 6 computer model, as described in Kneizys (11). LOWTRAN 6
was accessed through the Aeronautical Systems Division (ASD)
Cyber computer. In general, for standard atmospheric models, five
input cards are required to run the program for a given problem
(information required for the cards is inputted from a terminal).
If one of the additional models mentioned in Chapter 5 is used, a
combination of several of the ten additional control cards is
possible.

The formats for the five main cards and the additional cards
used is given below, along with the definition for each parameter
on the cards. Options that were used in this system are supplied,
while the details on other options available are given in Kneizys
(11:81-96).

Card 1
Format:
MODEL, ITYPE, IEMSCT, M1, M2, M3, IM, NOPRT, TBOUND, SALB

The parameter MODEL selects one of six geographical model
atmospheres or specifies that user-defined meteorological data
are to be used in place of the standard models. The option
selected for this system was the tropical model atmosphere. ITYPE

74

defines one of three types of atmospheric paths for a given problem. The option selected for this system was a vertical or slant path to space. IEMSCT selects the mode of program execution. The option selected was to calculate the transmittance. M1, M2, M3, IM, SALB, and TBOUND are additional input parameters for non-standard cases and were not used for this system. NOPRT is a user option to suppress printing of profiles and tables in the output.

Card 2

Format:

IHAZE, ISEASN, IVULCN, ICTSL, ICIR, IVSA, VIS, WSS, WHH, RAINRT

IHAZE, ISEASN, IVULCN, and VIS select the altitude and seasonal dependent aerosol profiles and aerosol extinction coefficients. IHAZE specifies the aerosol model used for the boundary layer (0 - 2 km) and a default surface meteorological range. The option used was for a maritime extinction. ISEASN selects the appropriate seasonal aerosol profile for both tropospheric and stratospheric aerosols, which for this system was set to the model default value. IVULCN controls both the selection of the aerosol profile as well as the type of extinction for the stratospheric aerosols, which for this system was set to the model default value. VIS is the surface meteorological range whose value for this system was determined by the IHAZE selection. ICSTL was not used in this system. ICIR

selects the inclusion of cirrus cloud attenuation in the calculation, and if used, is controlled by Card 2A. IVSA, WSS, and WHH were not used in this system. RAINRT is the rain rate, and was not used in this system.

Card 2A

Format:

CTHIK, CALT, ISEED

CTHIK is the cirrus thickness, CALT is the cirrus base altitude, and ISEED is the random number initialization flag. Default values were used for this system, which were a thickness of 1 km and a base altitude of 11 km.

Card 3

Format:

H1, H2, ANGLE, RANGE, BETA, RO, LEN

This card is used to define the geometrical path parameters. H1 is the initial altitude, H2 is the final altitude, ANGLE is the initial zenith angle measured from H1, RANGE is the path length, BETA is the earth centre angle subtended by H1 and H2, RO is the radius of the earth at a particular latitude, and LEN specifies the path. It is not necessary to specify every parameter; only those that adequately describe the problem. For

this system, only H1 and ANGLE were specified, and their values were varied to obtain the plots in Chapter 5.

Card 4

Format:

V1, V2, DV

This card specifies the spectral range and increment for the calculation. V1 is the initial frequency (in wavenumbers), V2 is the final frequency, and DV is the frequency increment.

Card 5

Format:

IRPT

The control parameter IRPT causes the program to recycle, so that a series of problems can be run with one submission of LOWTRAN.

Appendix B. Range and Angle Calculations

The following calculations refer to Figure 27. Point A is on the surface of the earth at the farthest distance from the satellite, and Point B is the satellite. O is the origin and the centre of the earth.
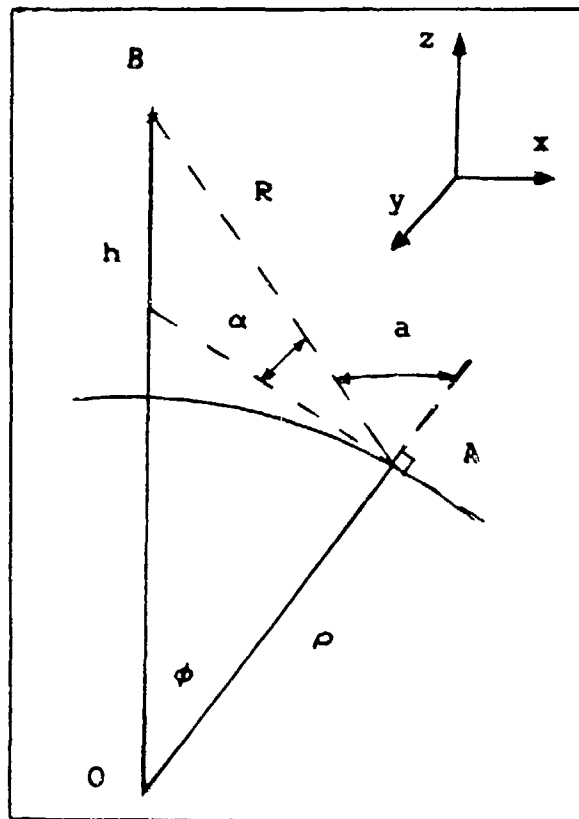

Figure 27. Angle and Range Reference Diagram

Converting spherical co-ordinates to rectangular co-ordinates

For <u>Point A.</u>

$$\rho = 6378 \text{ km} \qquad\qquad x_A = 1636.4 \text{ km}$$

$$\phi = 15 \text{ degrees} \qquad\qquad y_A = 215.4 \text{ km}$$

$$\theta = 7.5 \text{ degrees (not shown)} \qquad\qquad z_A = 6160.5 \text{ km}$$

For <u>Point B.</u>

$$x_B = 0 \text{ , } y_B = 0 \text{ , } z_B = 6378 + \text{Altitude h (km)}$$

$$\text{Range } R = \left[(x_A - x_B)^2 + (y_A - y_B)^2 + (z_A - z_B)^2 \right]^{1/2} \qquad (22)$$

To calculate the zenith angle for each altitude, change to two dimensions.

For <u>Point A.</u>

$$\rho = 6378 \text{ km} \qquad\qquad x'_A = 1650.7 \text{ km}$$

$$\phi = 15 \text{ degrees} \qquad\qquad z'_A = 6160.67 \text{ km}$$

The slope of the tangent to the earth's surface at Point A is

$$m_1 = -\frac{x'_A}{z'_A} = -0.2679$$

For <u>Point B.</u>

$$x_B = 0 \text{ , } z_B = 6378 + \text{Altitude h (km)}$$

The slope of the line $\overline{AB}$ is

$$m_2 = \frac{z_B - z'_A}{x_B - x'_A} = \frac{z_B - 6160.5}{-1650.75}$$

The angle between the line $\overline{AB}$ and the tangent to the surface is

$$\alpha = \tan^{-1}\left[\frac{m_2 - m_1}{1 + (m_2)(m_1)}\right] \qquad (23)$$

The zenith angle a is a = 90 - α (degrees)

Table 4 gives the ranges and zenith angles for various altitudes.

Table 4. Ranges and Zenith Angles for various Altitudes

Altitude h (km)	Range R (km)	Zenith Angle a (degrees)
300	1729.7	86.6
400	1762.2	84.5
500	1799.7	81.5
800	1938.9	73.4
1000	2050.9	68.6
1500	2382.1	58.9
2000	2764.3	51.7
2500	3179.5	46.3
3000	3616.2	42.2

BIBLIOGRAPHY

1. Bate, Roger B. and others. Fundamentals of Astrodynamics. New York : Dover Publications, 1971.

2. Boyd, J.A. and others. Electronic Countermeasures. Los Altos, CA : Peninsula Publishing, 1961.

3. Boyle, W.S. and G.E. Smith. "Charge Coupled Semiconductor Devices," Bell System Technical Journal, 49 : 587-593 (April 1970).

4. Bransom, Mikael A. Infrared Radiation : A Handbook for Applications. New York : Plenum Press, 1968.

5. Chan, William S. "Focal plane architecture: an overview," Proceedings of SPIE, 513 : 696-700. SPIE Press, 1985

6. Dereniak, Eustace L. and Devon G. Crowe. Optical Radiation Detectors. New York : John Wiley and Sons, 1984.

7. Haas, W.H., J.L. Rapier, F. Lee and C.R. Johnson. "Low power challenge to signal processing for space based mosaic sensors," Proceedings of SPIE, 311 : 91-99. SPIE Press, 1981

8. Henbest, Nigel. "Electronics show the Universe in a new light," New Scientist, 36 : 46-49. (March 1986).

9. Jamieson, John A. "Infrared technology: advances 1975-84, challenges 1985-94," Optical Engineering, 25 : 688-697. (May 1986).

10. KAF-1400. Full-Frame CCD Imager. Product Brochure. Eastman Kodak Company, Rochester NY, 1987.

11. Kneizys, F.X. and others. Atmospheric Transmittance/Radiance Computer Code LOWTRAN 6. Optical Physics Division, Air Force Geophysics Laboratory, Hanscom AFB MA, August 1983 (AD-A137786).

12. Kruer, M.R., D.A. Scribner and J.M. Killiany. "Infrared focal plane array technology development for Navy applications," Optical Engineering, 26 : 182-191. (March 1987).

13. Lange, James J. and Howard E. Evans. "Electro-Optical Space Systems Technology", Course Notes, PHYS 621 Electro-Optical Space Systems Technology. School of Engineering, Air Force Institute of Technology (AU), Wright-Patterson AFB OH, January 1987.

14. Lange, James J. and Howard E. Evans. "Elements of Remote Sensing", Course Notes, PHYS 521 Space Surveillance. School of Engineering, Air Force Institute of Technology (AU), Wright-Patterson AFB OH, October 1986.

15. Lloyd, Donal B. "Staring IR Sensors," Military Electronics/Countermeasures 18 : 58-95. (November 1979).

16. Neel, Riley. "Challenges in processing data from mosaic sensors," Proceedings of SPIE, 311 : 84-90. SPIE Press, 1981.

17. Schultz, James and David Russell. "New Staring Sensors," Defense Electronics 44-51. (July 1984).

18. Slater, Philip N. Remote Sensing : Optics and Optical Systems. London : Addison-Wesley Publishing Company, 1980.

19. Steckl, A.J. "Infrared Charge Coupled Devices," Proceedings of SPIE, 513 : 621-629. SPIE Press, 1985.

20. Tebo, Albert. "IR Detector Technology Part II," Laser Focus/Electro-optics 68-82. (July 1984).

21. Wolfe, William L. and George J. Zissis, Editors. The Infrared Handbook. Office of Naval Research, Department of the Navy, Washington D.C., 1978.

VITA

Flight Lieutenant Timothy J. Lawder was born on 19 July 1959 in Bristol, England. He graduated from High School in Townsville, Queensland (Australia) in 19▪▪. He joined the Royal Australian Air Force (RAAF) and attended the Royal Melbourne Institute of Technology, from which he received the degree of Bachelor of Engineering in Communication Engineering in May 1981. He was employed as a Base Radio Officer at Sale, Victoria for three years and then at RAAF Headquarters Support Command as the system support engineer for Air Defence Ground Equipment. He entered the School of Engineering, Air Force Institute of Technology, in May 1986.

    Permanent Address: Department of Defence (Air Force Office)
                         Russell Offices
                         Canberra
                         ACT, 2600
                         Australia

REPORT DOCUMENTATION PAGE			Form Approved OMB No. 0704-0188
1a. REPORT SECURITY CLASSIFICATION UNCLASSIFIED		1b RESTRICTIVE MARKINGS	
2a. SECURITY CLASSIFICATION AUTHORITY		3. DISTRIBUTION/AVAILABILITY OF REPORT Approved for public release; distribution unlimited.	
2b. DECLASSIFICATION/DOWNGRADING SCHEDULE			
4. PERFORMING ORGANIZATION REPORT NUMBER(S) AFIT/GSO/ENP/87D-1		5 MONITORING ORGANIZATION REPORT NUMBER(S)	
6a. NAME OF PERFORMING ORGANIZATION School of Engineering	6b. OFFICE SYMBOL (If applicable) AFIT/ENS	7a. NAME OF MONITORING ORGANIZATION	
6c. ADDRESS (City, State, and ZIP Code) Air Force Institute of Technology (AU) Wright-Patterson AFB, OH 45433-6583		7b. ADDRESS (City, State, and ZIP Code)	
8a. NAME OF FUNDING/SPONSORING ORGANIZATION	8b OFFICE SYMBOL (If applicable)	9 PROCUREMENT INSTRUMENT IDENTIFICATION NUMBER	
8c. ADDRESS (City, State, and ZIP Code)		10 SOURCE OF FUNDING NUMBERS	

10 SOURCE OF FUNDING NUMBERS			
PROGRAM ELEMENT NO	PROJECT NO	TASK NO	WORK UNIT ACCESSION NO

11 TITLE (Include Security Classification)
See Box 19

12 PERSONAL AUTHOR(S)
Timothy J. Lawder, B.E., FLTLT, RAAF

13a TYPE OF REPORT MS Thesis	13b TIME COVERED FROM _____ TO _____	14 DATE OF REPORT (Year, Month, Day) 1987 November	15 PAGE COUNT 95

16 SUPPLEMENTARY NOTATION

17 COSATI CODES			18 SUBJECT TERMS (Continue on reverse if necessary and identify by block number)
FIELD	GROUP	SUB-GROUP	Infrared Detection, Thermal Targets, Satellite Tracking Systems, Aircraft Detection
17	05	01	

19 ABSTRACT (Continue on reverse if necessary and identify by block number)

Title: SPECIFICATION FOR AN INFARED SATELLITE
SURVEILLANCE SYSTEM FOR THE DETECTION
OF AIRCRAFT

Thesis Advior: Howard E. Evans, Lt. Col., USAF
Instructor of Physics

20 DISTRIBUTION/AVAILABILITY OF ABSTRACT ☒ UNCLASSIFIED UNLIMITED ☐ SAME AS RPT ☐ DTIC USERS	21 ABSTRACT SECURITY CLASSIFICATION UNCLASSIFIED	
22a NAME OF RESPONSIBLE INDIVIDUAL Howard E. Evans, Lt. Col., USAF	22b TELEPHONE (Include Area Code) (513) 255 2012	22c OFFICE SYMBOL AFIT/ENP

DD Form 1473, JUN 86   Previous editions are obsolete   SECURITY CLASSIFICATION OF THIS PAGE

This report gives a methodology for designing an infrared satellite surveillance system for detection of aircraft against a background of the earth. Values for target intensity and background radiance have been assumed, and a satellite focal plane array configuration has been designed. System calculations have been performed and indicate that detection of aircraft against a background of the earth appears feasible. This report contains limited actual data due to its unclassified level.